國 立 交 通 大 學

電子工程學系 電子研究所碩士班

碩 士 論 文

射頻前端接收器設計

RF Front-end Receiver Design

研 究 生：蔡 順 意

指導教授：胡 樹 一 博 士

中 華 民 國 九 十 六 年 十 一 月

射頻前端接收器設計

RF Front-end Receiver Design

研 究 生 : 蔡 順 意   Student: Shun-I Tsai

指導教授 : 胡 樹 一 博 士   Advisor: Dr. Robert Hu

國 立 交 通 大 學

電 子 工 程 學 系 電 子 研 究 所 碩 士 班

碩 士 論 文

A Thesis
Submitted to Department of Electronics Engineering & Institute of Electronics
College of Electrical and Computer Engineering
National Chiao Tung University
in Partial Fulfillment of the Requirements
for the Degree of Master
In
Electronics Engineering
2007
HsinChu, Taiwan, Republic of China

中華民國 九十六 年 十一 月

國 立 交 通 大 學

博碩士論文全文電子檔著作權授權書

（提供授權人裝訂於紙本論文書名頁之次頁用）

本授權書所授權之學位論文，為本人於國立交通大學 __電子工程學__ 系所 __乙__ 組， __九十六__ 學年度第_一_學期取得碩士學位之論文。

論文題目：**RF Front-end Receiver Design**

指導教授：**胡 樹 一 博 士**

■ 同意　□不同意

本人茲將本著作，以非專屬、無償授權國立交通大學與台灣聯合大學系統圖書館：基於推動讀者間「資源共享、互惠合作」之理念，與回饋社會與學術研究之目的，國立交通大學及台灣聯合大學系統圖書館得不限地域、時間與次數，以紙本、光碟或數位化等各種方法收錄、重製與利用；於著作權法合理使用範圍內，讀者得進行線上檢索、閱覽、下載或列印。

論文全文上載網路公開之範圍及時間：	
本校及台灣聯合大學系統區域網路	■ 中華民國一百年一月一日公開
校外網際網路	■ 中華民國一百年一月一日公開

授 權 人：蔡 順 意

親筆簽名：_蔡 順 意_

中華民國　九十六　年　十一　月　二十九　日

射 頻 前 端 接 收 器 設 計

研究生 : 蔡順意　　　　　指導教授 : 胡樹一 博 士

國立交通大學

電子工程學系　電子研究所碩士班

摘要

　　本篇論文提出一個 4GHz 到 20GHz 的低雜訊寬頻放大器，和一種新穎被動式混波器。低雜訊寬頻放大器是運用 4 顆電晶體，接成共源極的架構；利用輸入閘極電感和並聯回授電容，來完成輸入阻抗匹配。整體放大器在工作頻率範圍，功率增益可達 22 dB，輸入反射係數低於 -10dB。最後在臺灣基體電路公司下線，使用 0.18 微米互補性氧化金屬半導體製程。被動式混波器是一種全新的架構，從未被發表在國際期刊。這個架構沒有直流功率消耗，沒有 1 dB 功率抑制點；在沒有濾波器的情形下，輸出中頻的載波和射頻訊號可被有效消除。

RF Front-end Receiver Design

Student: Tsai Shun-I   Advisor: Dr. Robert Hu

Department of Electronic Engineering &
Institute of Electronics
National Chiao Tung University

Abstract

This thesis presents a 4GHz to 20GHz low noise amplifier, and a novel architecture of mixer. Low noise amplifier utilizes four MOS transistors which are designed as common-mode source architecture, and apply gate inductor and parallel-feedback capacitor to achieve wide-band input impedance matching. Power gain can be up to 22dB and input reflection coefficient can be lower than -10dB on intended frequency range, and is fabricated in TSMC 0.18μm CMOS technology. The passive mixer is a novel architecture, and is never published on worldwide international papers. This architecture doesn't consume any DC power and no 1-dB compression issue. Besides, at IF output terminal, LO and RF signals can be effectively eliminated without any filters.

致謝

感謝胡樹一老師三年來的教導，無論在研究上或其他方面，老師真的很感謝您。謝謝 319 實驗室博士班學長 Fadi，他在 ADS 上的指導；謝謝本實驗室全體同學適時的幫助。最後要感謝父母背後的支持，讓我全心全意完成學業，謝謝。

Table of Contents

Figure Captions

Chapter 1
Introduction

1.1 Motivation

In modern life, the distance between people and people is getting shorter and shorter, and people are easy to gather any kind of messages. It is attributed to technology advanced and numerous commercial communication products are presented to public, such as cellular phone [1-4], wireless LAN [5-9], Bluetooth headset [10], GPS, ZigBee [11], WiMAX, xDSL devices, …. and so forth. Most of them have the capability of wireless to transmit and receive different information. Besides, even more wireless techniques are put on scientific applications, such as astronomical telescope. Therefore, wireless technology is playing a significant role in our daily life, and gradually altering our life style.

In a progressive wireless communication system, there are several characteristics making the system deliver and receive signals much more efficient. The First one, a high efficient antenna is essential. Under the help of a high efficient antenna, an electromagnetic wave can be propagated much father, and much weaker signals can be received. The second one is low noise amplifier, being named as LNA for short. LNA is usually placed in the receiving signals path in a wireless communication system. After signals are fetched from free air by antenna, they are usually directly delivered to LNA for increasing the sensitiveness of system. With LNA's assistances, the system can process much more fragile signals, and greatly enhance the performance of whole communication system [12-13]. The third one is mixer, it is responsible for frequency conversion. Owing to the dimension of antenna is direct proportional to signal's wave length. Hence, in a wireless communication

system, the dimension of antenna could be unrealizable without frequency conversion. Mixer always processes the signal amplified by LNA, and combine radio frequency signal and local oscillation signal to generate intermediate frequency signal. The simplest mixer is like a switch. It turns on and off the signal path of radio frequency. Consequently, mixer always brings much noises which might make the system has the troubles on demodulation [14]. The fourth one is power amplifier [15], it is always located in the signal transmission path. After the transmitted signals get modulated and before sent to antenna, the adequate amplification is required for enlarging the range of communication distance. The last one is suitable modulation technique [16-17]. A high performance modulation skill makes communication systems deliver and receive a huge amount of information in a short time. The most popular modulation skill in modern world is OFDM plus spread spectrum technique. OFDM treats one signal path as multiple channels. The signal in each channel is usually modulated in QAM. The spread spectrum skill is an outstanding invention in the recent twenty years. It makes it become possible that the power level of radio frequency signals lower than the one of noise power.

From above descriptions, a wireless communication system is pretty interesting, but very complicated. In this thesis, only LNA and mixer are studied. A 4G to 20GHz LNA is simulated and implemented in a standard $0.18\,\mu$m CMOS technology. A passive mixer with very low intermodulation is designed and simulated in Agilent Advanced Design System 2003A.

1.2   A Brief Wireless History

Wireless communication technologies have existed and been utilized for more than a hundred years. Guglielmo Marconi, the Italian founder of wireless technologies, developed an interest in technology and communications as a child. He had read about and understood the work

of Heinrich Rudolf Hertz and began to see the significance that wireless communication would have for the modern world. In 1894 Marconi began experimentations, and in 1899 sent a telegraphic message across the English Channel without any cables. Only three years later, Marconi's wireless devices were able to send and receive a telegraph across the Atlantic Ocean.

Fig. 1.1   Marconi System

In the early years of Marconi's wireless telegraphy, the main uses for it were for military purposes. The first war that Marconi's wireless communications systems were used was the Boer War in 1899, and in 1912, a wireless device set sail with the Titanic. It was the best system in the world, and without it, the tragedy of the Titanic could have been worse, because it was the device that alerted other ships in the area of the sinking Titanic. By the 1920s, wireless telegraphy had become a mass medium, and its popularity soared with the public's discovery that it could send personal messages across continents. With the introduction of broadcast radio, wireless technology became commercially viable.

In the last thirty years wireless communication technologies have seen a revolution, as people rediscover the uses for it, and its advantages.

In the 1980s, wireless technologies were analogue signals (1G), in the 1990s they changed to digital (2G), recently they remained digital but became better quality and faster, and now the future is heading rapidly for 4G communications. In 1994, the Ericsson telecommunications company began devising and developing a technology that would connect portable devices whilst replacing cables. They named this device as Bluetooth after King Harald I of Norway, who joined Denmark and Norway. Under the aims of the Ericsson company for Bluetooth, this parallel the objective of Bluetooth technology, which aims to unite the computer and telecommunication industry. After its initial development, Ericsson realized that the product had huge potential worldwide, and from the Bluetooth Special Interest Group, which now includes over 1000 companies from around the world. The demand on today's society has seen technologies like Bluetooth becoming an extremely popular alternative to wired communications and cables.

1.3   Introduce to The Standards on Wireless Communication System

1.3.1   Wi-Fi

Wi-Fi is short for wireless fidelity and is meant to be used generically when referring of any type of 802.11 network, whether 802.11b, 802.11a, dual-band, etc. The term is promulgated by the Wi-Fi Alliance. Any products tested and approved as "Wi-Fi Certified" (a registered trademark) by the Wi-Fi Alliance are certified as interoperable with each other, even if they are from different manufacturers. A user with a "Wi-Fi Certified" product can use any brand of access point with any other brand of client hardware that also is certified. Typically, however, any Wi-Fi product using the same radio frequency (for example, 2.4GHz for 802.11b or 11g, 5GHz for 802.11a) will work with any other,

even if not "Wi-Fi Certified."

Formerly, the term "Wi-Fi" was used only in place of the 2.4GHz 802.11b standard, in the same way that "Ethernet" is used in place of IEEE 802.3. The Alliance expanded the generic use of the term in an attempt to stop confusion about wireless LAN interoperability.

An 802.11 LAN is based on a cellular architecture where the system is subdivided into cells, where each cell (called **Basic Service Set** or **BSS**, in the 802.11 nomenclature) is controlled by a Base Station (called **Access Point**, or in short **AP**).

Even though that a wireless LAN may be formed by a single cell, with a single Access Point, (and as will be described later, it can also work without an Access Point), most installations will be formed by several cells, where the Access Points are connected through some kind of backbone (celled **Distribution System** or **DS**), typically Ethernet, and in some cases wireless itself.

The whole interconnected Wireless LAN including the different cells, their respective Access Points and the Distribution System, is seen to the upper layers of the OSI model, as a single 802 network, and is called in the Standard as **Extended Service Set** (**ESS**).

The following picture shows a typical 802.11 LAN, with the components described previously:
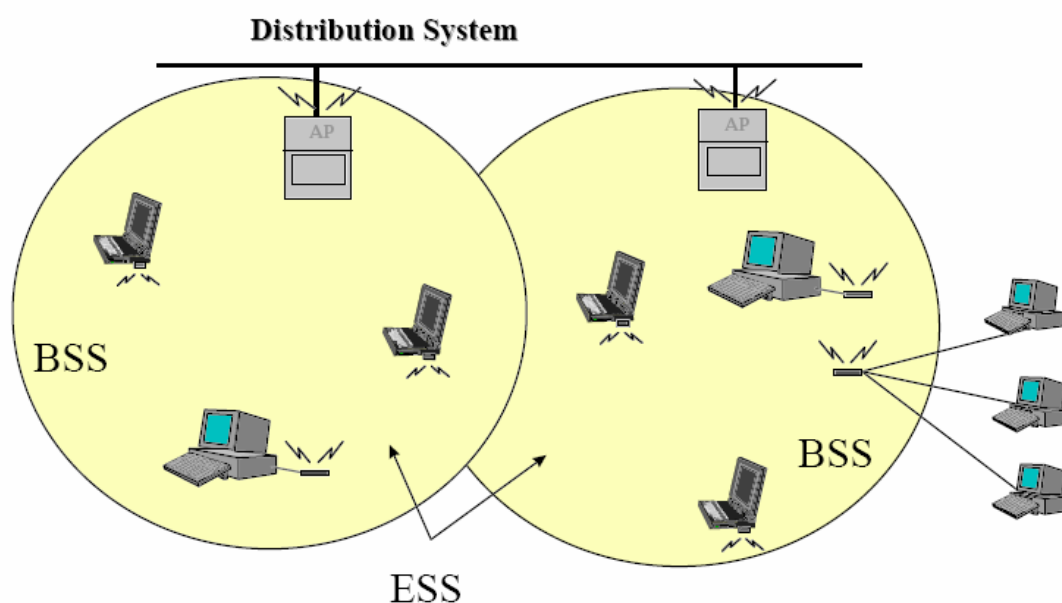
Fig. 1.2   The typical Architecture of 802.11 LAN

1.3.1 BlueTooth

In early 1998, a consortium of companies including Ericsson, IBM, Intel, Nokia, and Toshiba formed a special interest group, codenamed "Bluetooth". The group's goal was to develop a low-cost, flexible wireless platform for short-distance communication (< ~10 meters). The Bluetooth 1.0 specifications were released on July 26, 1999, but the technology has only recently become cheap enough for widespread use. The cost of a Bluetooth radio chip has dropped from $20 and is now approximately $5.

Spectrum is divided up into 79 channels spaced 1 MHz apart. Data is transmitted at 1 Mbps. For security benefits and noise reduction, a Bluetooth transmitter employs frequency hopping, switching channels up to 1600 times a second.

Bluetooth is capable of point-to-point or point-to-multipoint communication. This flexibility allows Bluetooth to be used in a wide variety of applications. Because power consumption is always a concern for mobile devices, Bluetooth has three power classes that can be used depending on how far apart the communicating devices are from one another.

In 2002 Ericsson's Bluetooth technology had finally won a standard with the IEEE global standards body, a much needed shot in the arm for the fledgling wireless Personal Area Network (PAN) technology. The standard, 802.15.1, will lend validity to Bluetooth devices, and enable vendors to better support the hardware and software involved. Bluetooth devices based on this standard will suffer fewer compatibility issues than current implementations.

The IEEE licenses part of the current standard, authored by the Bluetooth SIG, as a basis for its 802.15 standard. As a result, 802.15 devices will be fully compatible with Bluetooth v1.1 devices.

Over the next few years, Bluetooth's use is expected to significantly grow. The specifications for Bluetooth 2.0 had been finalized for a couple years. Bluetooth 2.0 had been designed to complement existing Bluetooth devices and will offer data transmission rates up to 12 Mbps.

Chapter 2

The Principal Concepts of

Designing Low Noise

Amplifier and Mixer

In this chapter, the principal concepts on designing Low Noise Amplifier and Mixer will be introduced. Since RF receiving front-end circuits usually get extremely weak signals from free space. The extremely weak signals are susceptible to noise, and always greatly affect overall performance. Therefore, before we begin to design RF receiving front-end circuits, the most important thing for us is to realize why noise is generated, and how to reduce the effect of noise. Besides, while designing each block such as LNA, mixer, we should have system view for acquiring the best overall performance. Hence, some design considerations and characteristics will be carefully taken into account in this chapter.

2.1   Introduction Noise Sources

In this subsection, only the intrinsic noises will be introduced. They are caused by small current and voltage fluctuations produced within devices themselves. The extraneous man-made signals that could be a problem in high-gain circuit will be excluded. The existence of noise is basically due to the fact that electrical charge is not continuous, and the

discrete amount is equivalent to electron charge.

The study of noise is important because it represents a lower limit to the size of electric signal that can be amplified by a circuit without significant deterioration in signal quality. Noise also results in an upper limit to the useful gain of amplifier, because if the gain is increased without limit, the output stage of the circuit eventually begins to enter saturated region.

2.1.1 Shot Noise

Shot noise is always taken place in diodes, bipolar transistors and MOSFETs, and has relations with the conduct current on them. The origin of shot noise can be seen by considering the carrier concentrations in a diode biased in forward region. An electrical file ξ exists in the depletion region and a voltage ($\phi_0 - V$) exists between the p-type and n-type regions, where ϕ_0 is the build-in potential and V is the forward bias on the diode. The forward current of the diode I is composed of holes from the p region and electrons from n region, which have sufficient energy to overcome the potential barrier at the junction. Once the carriers have crossed the junction, they diffuse away as minority carriers.

The passage of each carrier across the junction, which can be modeled as a random event, is dependent on the carrier having sufficient energy and a velocity directed toward the junction. Thus external current I, which appears to be a steady current, contains a large number of random independent current pulses. If the current is examined on a sensitive oscilloscope, the trace appears as Fig. 2.1, where I_D is the average current.
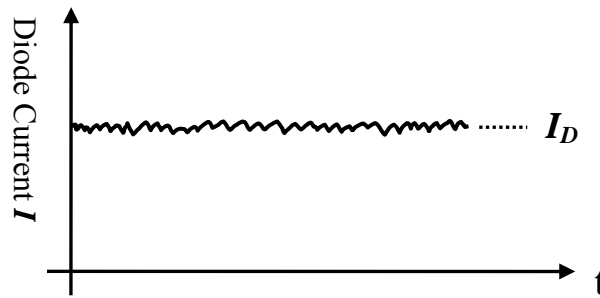
Fig. 2.1 Diode current I as a function of time

The fluctuation in **I** is termed *shot noise* and is generally specified in terms of its mean-square variation about average value. This is written as $\overline{i^2}$, where

$$
\begin{aligned}
\overline{i^2} &= \overline{(I - I_D)^2} \\
&= \lim_{T \to \infty} \frac{1}{T} \int_o^T (I - I_D)^2 dt
\end{aligned}
\tag{2.1}
$$

It can be shown that if a current **I** is composed of a series of random independent pulses with average value **I**$_D$, then the resulting noise current has a mean-square value

$$
\overline{i^2} = 2qI_D\Delta f
\tag{2.2}
$$

Where **q** is the electronic charge (1.6×10^{-19}C) and Δf is the bandwidth in hertz. This equation shows that the noise current has a mean-square value that is directly proportional to the bandwidth Δf (in hertz) of the measurement. Thus a noise-current spectral density $i^2/\Delta f$ (with units square amperes per hertz) can be defined that is constant as a function of frequency.

2.1.2 Thermal Noise

The mechanism producing thermal noise is totally different from

shot noise. In conventional resistors it is due to the random thermal motion of the electrons and is unaffected by the presence or absence of direct current, since typical electron drift velocities in a conductor are much less than electron thermal velocities. Since this source of noise is due to the thermal motion of electrons, we expect that it is related to absolute temperature T. In fact thermal noise is directly proportional to T (unlike shot noise, which is independent of T), as T approaches zero, thermal noise approaches zero.

In a resistor R, thermal noise can be shown to be represented by series voltage generator as shown in Fig. 2.2a, or by a shunt current generator $\overline{i^2}$ as in Fig. 2.2b. These representations are equivalent and

$$\overline{v^2} = 4kTR\Delta f \tag{2.3}$$

$$\overline{i^2} = 4kT\frac{1}{R}\Delta f \tag{2.4}$$

Where k is Boltzmann's constant. At room temperature $4kT = 1.66 \times 10^{-20}$ V-C. Equation 2.3 and 2.4 show that the noise spectral density is again independent of frequency and, for thermal noise, this is true up to 10^{13} Hz. Thus thermal noise is another source of white noise. Note that the Norton equivalent of 2.4 can be derived from 2.3 as

$$\overline{i^2} = \frac{\overline{v^2}}{R^2} \tag{2.5}$$

A useful number to remember for thermal noise is that at room temperature (300 ˚K), the thermal noise spectral density in a 1-K Ω resistor is $\overline{v^2}/\Delta f \approx 16 \times 10^{-18}$ V^2/Hz. Another useful equivalence is that the thermal noise-current generator of a 1-K Ω resistor at room temperature is the same as that of 50μA of direct current exhibiting shot noise.

Thermal noise as described above is a fundamental physical phenomenon and is present in any linear passive resistor. This includes conventional resistors and the radiation resistance of antennas, loudspeakers, and microphones. In the case of loudspeakers and microphones, the source of noise is the thermal motion of the air

molecules.In the case of antennas, the source of noise is the black-body radiation of the object at which the antenna is directed. In all cases, (2.3) and (2.4) give the mean-square value of the noise.
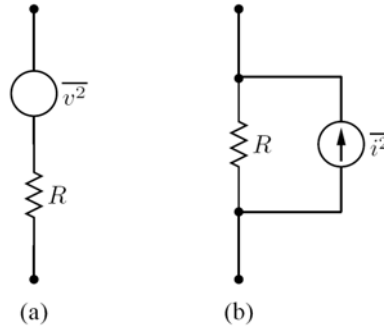
Fig. 2.2   Alternative of Thermal Noise

2.1.3   Flicker Noise

Flicker noise in one of noise found in all active device, as well as in some discrete passive elements such as carbon resistors. The origins of flicker noise are varied, but it is caused mainly by traps associated with contamination and crystal defects. These traps capture and release carriers in a random fashion and the time constants associated with the process give rise to a noise signal with energy concentrated at low frequencies.

Flicker noise, which is always associated with a flow of direct current, displays a spectral density of the form

$$\overline{i^2} = K_1 \frac{I^a}{f^b} \Delta f \qquad (2.6)$$

where

$$\Delta f \;\; = \;\; \text{small bandwidth at frequency } f$$
$$I \;\; = \;\; \text{direct current}$$
$$K_1 \;\; = \;\; \text{constant for a particular device}$$
$$a \;\; = \;\; \text{constant in the range 0.5 to 2}$$
$$b \;\; = \;\; \text{constant of about unity}$$

If b = 1 in (2.6), the noise spectral density has a *1/f* frequency dependence (hence the alternative name *1/f* noise), as shown in Fig. 2.3. It is apparent that flicker noise is most significant at low frequencies,

although in devices exhibiting high flicker noise levels, this noise source may dominate the device noise at frequency well into the megahertz range.
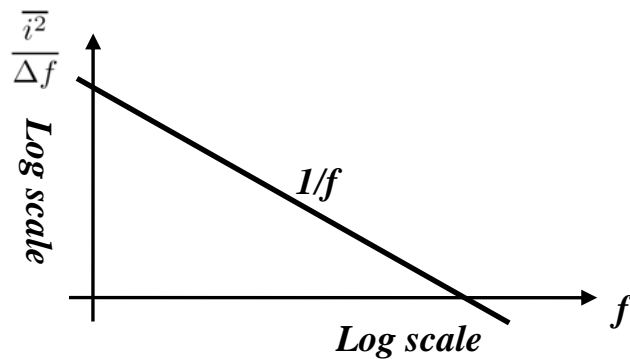

Fig. 2.3   Flicker Noise spectral density versus frequency

It was noted above that flicker noise only exists in association with a direct current. Thus in the case of carbon resistors, no flicker noise is present until a direct current is passed through the resistor (however, thermal noise always exists in the resistor and is unaffected by any direct current as long as the temperature remains constant). Consequently, carbon resistors can be used if required as external elements in low-noise, low-frequency integrated circuits as long as they carry no direct current. If the external resistors for such circuits must carry direct current, however, metal film resistors that have no flicker noise should be used.

The final characteristic of flicker noise that is of interest is its amplitude distribution, which is often non-Gaussian.

2.1.4   Burst Noise

Burst noise is another type of low-frequency noise found in some integrated circuits and discrete transistors. The source of this noise is not fully understood, although it has been shown to be related to the presence of heavy-metal ion contamination. Gold-doped device show very high levels of burst noise.

Burst noise is so named because an oscilloscope trace of this type

of noise shows burst of noise on a number (two or more) of discrete levels. The repetition rate of the noise pulses is usually in the audio frequency range (a few kilohertz or less) and produces a popping sound when played through a loudspeaker. This has led to the name popcorn noise for this phenomenon.

The spectral density of burst noise can be shown to be the form

$$\overline{i^2} = K_2 \frac{I^c}{1 + (\frac{f}{f_c})^2} \Delta f \tag{2.7}$$

where

K_2 = constant for a particular device
I = direct current
c = constant in the range 0.5 to 2
f_c = particular frequency for a given noise process

The spectrum is plotted in Fig. 2.4 and illustrates the typical hump that is characteristic of burst noise. At higher frequencies the noise spectrum falls as $1/f^2$. Burst noise processes often occur with multiple time constants, and this gives rise to multiple humps in the spectrum. Also flicker noise in invariably present as well so that the composite low-frequency noise spectrum often appear as in Fig. 2.5. As with flicker noise, factor K_2 for burst noise varies considerably and must be determined. The amplitude distribution of the noise is also non-Gaussian.
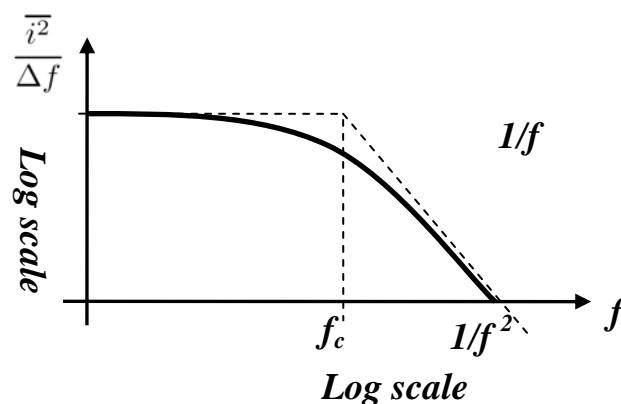

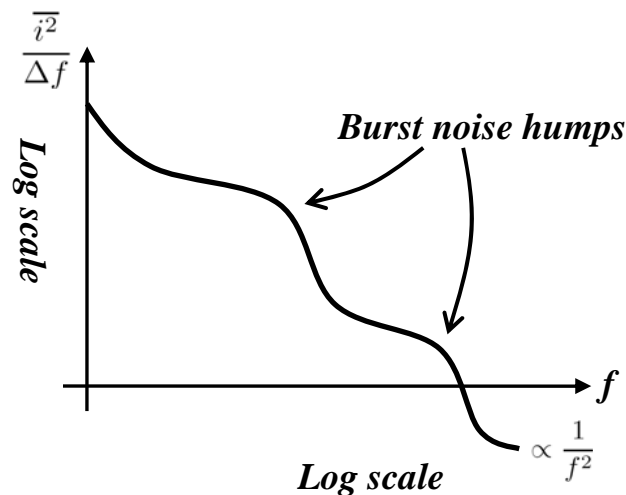Fig. 2.4 Burst Noise spectral density versus frequency

Fig. 2.5   Spectral density of combined multiple burst noise sources and flicker noise.

2.1.5   Avalanche Noise

Avalanche noise is a form of noise produced by Zener or avalanche breakdown in a *pn* junction. In avalanche breakdown, holes and electrons in the depletion region of a reverse-biased *pn* junction acquire sufficient energy to create hole-electron pairs by colliding with silicon atoms. This process is cumulative, resulting in the production of a random series of large noise spikes. The noise is always associated with a direct-current flow, and the noise produced is much greater than shot noise in the same current, as given by (2.2). This is because a single carrier can start an avalanching process that results in the production of a current burst containing many carriers moving together. The total noise is the sum of a number of random bursts of this type.

The most common situation where avalanche noise is a problem occurs when Zener diodes are used in the circuit. These devices display avalanche noise and are generally avoided in low-noise circuits. If Zener diodes are present, the noise representation of Fig. 2.6 can be used, where the noise is represented by a series voltage generator v^2. The dc voltage V_z is the breakdown voltage of the diode, and the series resistance R is

typically 10 to 100 Ω. The magnitude of $\overline{v^2}$ is difficult to predict as it depends on the device structure and the uniformity of the silicon crystal, but a typical measured value is $\overline{v^2}/\Delta f \approx 10^{-14}$ V^2/Hz at a dc Zener current of 0.5 mA. Note that this is equivalent to the thermal noise voltage in a 600-kΩ resistor and completely overwhelms thermal noise in **R**. The spectral density of the noise is approximately flat, but the amplitude distribution is generally non-Gaussian.
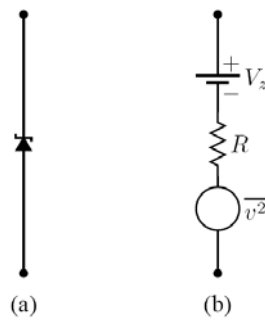

(a)   (b)

Fig. 2.6   Equivalent circuit of a Zener diode including noise

2.2   The Principal Concepts of Low Noise Amplifier

In a classical radio receiver, low noise amplifier is the most significant component, owing to it dominates the sensitivity of overall system [12]. The principal concepts of designing low noise amplifier are to compromise among input impedance, noise figure, power gain, power consumptions and linearity [11]. However, there are usually some tradeoffs among them, and there is almost not one circuit achieving all goals simultaneously, especially in ultra-wide band design. Besides, different process technology will influence the difficulty of goals' achievement. InP-BASED high electron-mobility transistor (HEMTs) provides an outstanding low-noise performance and superior high-frequency performance [18]. Moreover, HEMTs have excellent low-temperature performance, and do not have the carrier freeze-out effect even at temperature as low as 15K. However, compared with silicon technology, HEMT technology is very expensive. It is not suitable for commercial products. CMOS technology offers advantages such as low cost, mature process, good thermal conductivity, and large scale integration. However, CMOS technology suffers from high noise figure.

There are a huge number of papers published regarding low noise amplifier design. They were applying various structures for different applications. The resistive feedback amplifier [19] could easily achieve input impedance matching, yet it suffers from noise figure deterioration problem. Moreover, it usually limits input match at higher frequency due to the parasitic input capacitance [20]. The series feedback with inductive source degeneration [21-22] offers good input impedance with sufficient low noise figure, yet it is laborious for ultra-wide band design. The low noise amplifier employing an input three-section band-pass Chbyshev filter [20] can acquire wide band input impedance and low noise figure as well. However, the capacitance C_p between the gate and the source of the input device should be chosen considering the compromise between the size of L_s and the available power gain, while large C_p leads to the gain reduction due to the degradation of the effective cutoff frequency.

Below are three popular low noise amplifier structures which are widespread used in numerous products.

2.2.1　Classical Noise Matching Technique

Classical Noise Matching (CNM) Technique is used to acquiring minimum NF, F_{min}, by presenting the optimum noise impedance Z_{opt} to the given amplifier. We usually implement this technique by placing a matching circuit between the source and input of the amplifier. By applying this technique, the LNA can be designed to achieve an NF equal to F_{min} of the transistor, the lowest NF that can be obtained with the given technology. However, due to the inherent mismatch between Z_{opt} and Z^*_{in} (where Z^*_{in} is the complex conjugate of the amplifier input impedance), the amplifier can experience a significant gain mismatch at the input. Therefore, the CNM technique typically requires compromise between the gain and noise performance.

Fig. 2.7(a) shows a cascade-type LNA topology, which is one of the most popular topology due to its wide bandwidth, high gain, and high reverse isolation. In the given example, the selection of the cascade topology simplifies the analysis, and the gate-drain capacitance can be neglected.

Fig. 2.7(b) shows the simplified small-signal equivalent circuit of the cascade amplifier for the noise analysis including the intrinsic transistor noise model. In Fig. 2.7(b), the effects of the common-gate transistor M_2 on the noise and frequency response are neglected, as well as the parasitic resistances of gate, body, source, and drain terminal.

In Fig 2.7(b), $\overline{i_{nd}^2}$ represents the mean-squared channel thermal noise current, which is given by

$$\overline{i_{nd}^2} = 4kT\gamma g_{d0}\Delta f \tag{2.8}$$

Where g_{d0} is the drain-source conductance at zero drain-source voltage V_{DS}, k is the Boltzmann constant, T is the absolute temperature, and Δf is the bandwidth, respectively. The parameter γ has a value of unity at

zero V_{DS} and 2/3 in saturation mode operation with long channel devices. The value of γ increase at high V_{GS} and V_{DS} and can be more than two in short-channel devices.
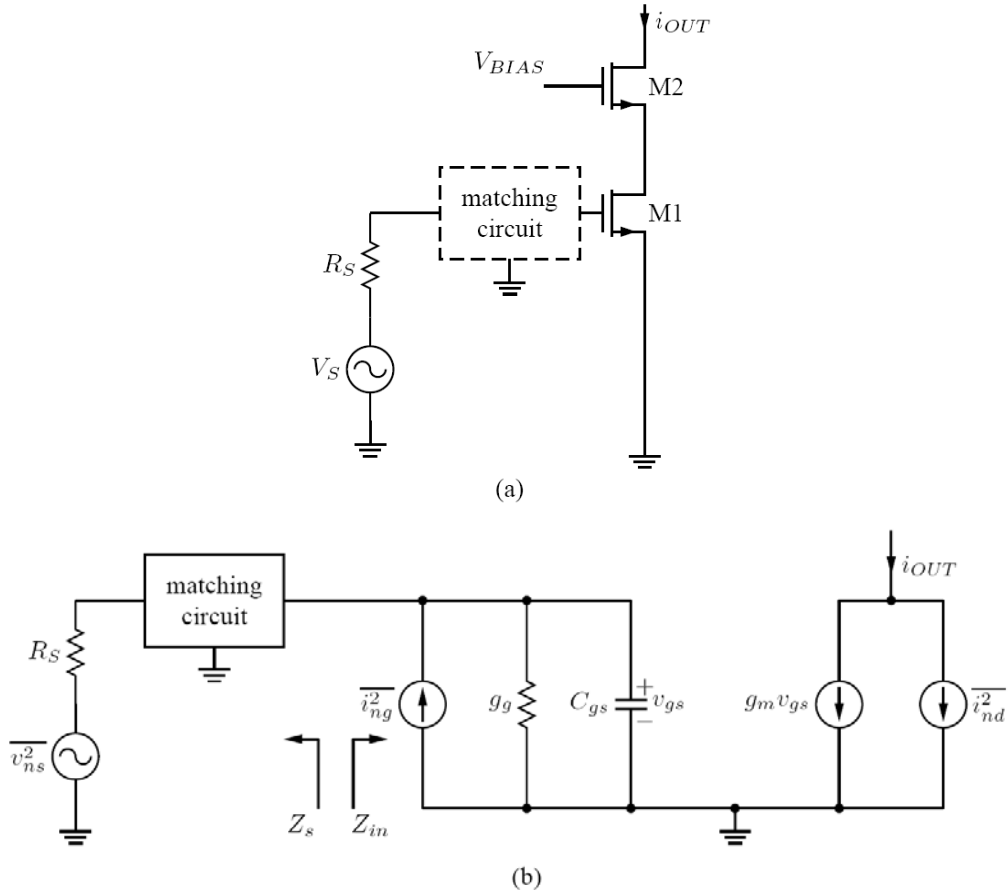

(a)

(b)

Fig. 2.7   (a)Schematic of a cascade LNA topology adopted to apply the CNM technique. (b) Its small-signal equivalent circuit.

The fluctuating channel potential due to channel noise current shown in (2.8) couples capacitively into the gate terminal, leading to a noisy gate current. The mean-squared gate-induced noise current is given by

$$\overline{i_{ng}^2} = 4kT\delta g_g \Delta f \tag{2.9}$$

where

$$g_g = \frac{\omega^2 C_{gs}^2}{5g_{d0}} \tag{2.10}$$

In (2.9), δ is a constant with value of 4/3 in long-channel device,

and C_{gs} represents the gate-source capacitance of the input transistor. Like γ, the value of δ also increases in short-channel devices and at high V_{GS} and V_{DS}. Since the gate-induced noise current has a correlation with the channel noise current, a correlation coefficient is defined as follows:

$$c = \frac{\overline{i_{ng} \times i_{nd}^*}}{\sqrt{\overline{i_{ng}^2}} \times \sqrt{\overline{i_{nd}^2}}} \tag{2.11}$$

After some lengthy algebraic derivations, the noise parameters for the cascode amplifier shown in Fig. 2.7(1) can be expressed as

$$R_n^0 = \frac{\gamma}{\alpha} \frac{1}{g_m} \tag{2.12}$$

$$Y_{opt}^0 = \alpha \omega C_{gs} \sqrt{\frac{\delta}{5\gamma}(1 - |c|^2)} - sC_{gs}\left(1 + \alpha|c|\sqrt{\frac{\delta}{5\gamma}}\right) \tag{2.13}$$

$$F_{min}^0 = 1 + \frac{2}{\sqrt{5}} \frac{\omega}{\omega_T} \sqrt{\gamma\delta(1 - |c|^2)} \tag{2.14}$$

where R_n^0 represents the noise resistance, Y_{opt}^0 is the optimum noise admittance, and F_{min}^0 is the minimum noise factor, respectively.

Note that, from Fig. 2.7(b), the input admittance is purely capacitive, i.e., $Y_{in}^0 = j\omega C_{gs}$. By comparing the complex conjugate of Y_{in}^0 with (2.13), it can be seen that the optimum source admittance for input matching is inherently different from that of the noise matching in both real and imaginary part. Thus, with the given example, one cannot obtain input matching and minimum NF simultaneously. This is the main limitation of the CNM technique when applied to the LNA topology shown in Fig. 2.7(a).

2.2.2 Simultaneous Noise and Input Matching Technique

While designing low noise amplifier, feedback techniques are always implemented in order to shift the optimum noise impedance Z_{opt} to the desired point. Shunt feedback has been applied for wide-band [23] and better input/output matching. Series feedback has been preferred to

obtain SNIM without the degradation of the NF. The series feedback with inductive source degeneration, which is applied to the common-source or cascode topology, is especially widely used for narrow-band applications.

Fig. 2.8(a) and (b) shows a cascade LNA with inductive source degeneration and the simplified small-signal equivalent circuit.
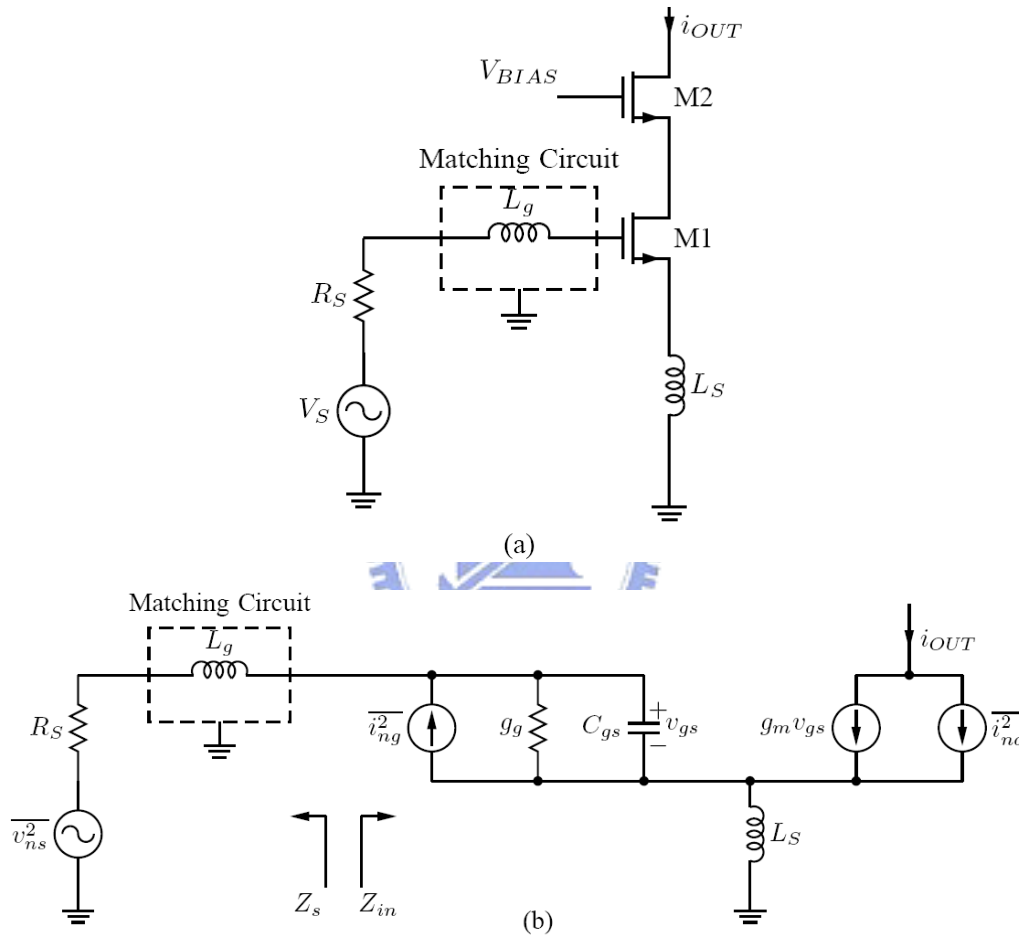

Fig. 2.8   (a) Schematic of a cascode LNA topology adopted to apply the SNIM technique. (b) Its small-signal equivalent circuit.

In Fig. 2.8(b), the same simplifications are applied as in Fig. 2.7(b). The following are the ways to obtain the noise parameter expressions of a MOSFET with series feedback: noise transformation formula using noise parameters, using the noise matrix, or Kirchoff's current las/Kirchoff's voltage law (KCL/KVL) with noise current sources. As in (2.12)-(2.14), the noise parameters seen in the gate of the circuit shown in Fig. 2.8(b)

can be obtained. The derivation is somewhat tedious, but the result is simple enough to provide useful insights. The noise factor and noise parameters can be given by

$$F = 1 + \frac{1}{g_m^2 R_s} \cdot \left\{ \gamma g_{d0} \cdot \left\{ \left[1 + s^2 C_{gs}(L_g + L_s)\left(1 + |c|\alpha\sqrt{\frac{\delta}{5\gamma}}\right) \right]^2 \right. \right.$$

$$- (sC_{gs}R_s)^2 \left(1 + |c|\alpha\sqrt{\frac{\delta}{5\gamma}}\right)^2 \right\}$$

$$\left. - \frac{\alpha\delta}{5}(1 - |c|^2)g_m(sC_{gs})^2(R_s^2 - sL_g^2) \right\} \qquad (2.15)$$

$$R_n = R_n^0 = \frac{\gamma}{\alpha}\frac{1}{g_m} \qquad (2.16)$$

$$Z_{opt} = Z_{opt}^0 - sL_s \qquad (2.17)$$

$$F_{min} = F_{min}^0 = 1 + \frac{2}{\sqrt{5}}\frac{\omega}{\omega_T}\sqrt{\gamma\delta(1 - |c|^2)} \qquad (2.18)$$

In (2.16)-(2.18), the noise parameters with superscripted zeros are those of the cascode amplifier with no degeneration [see (2.12)-(2.14)]. Note that (2.17) is expressed in impedance, as it is simpler in this case, and Z_{opt}^0 is given by

$$Z_{opt}^0 = \frac{1}{Y_{opt}^0} = \frac{\alpha\sqrt{\frac{\delta}{5\gamma(1-|c|^2)}} + j\left(1 + \alpha|c|\sqrt{\frac{\delta}{5\gamma}}\right)}{\omega C_{gs}\left\{ \sqrt{\frac{\alpha^2\delta}{5\gamma(1-|c|^2)}} + \left(1 + \alpha|c|\sqrt{\frac{\delta}{5\gamma}}\right)^2 \right\}} \qquad (2.19)$$

Note that, from (2.16)-(2.18), only Z_{opt} is shifted and there is no change in R_n and F_{min}. Also, note that (2.16)-(2.18) are valid for any arbitrary matching circuits, as well as the source impedance R_s in Fig. 2.8. In addition, as shown in Fig. 2.8(b), the input impedance Z_{in} of the given LNA can be expressed as

$$Z_{in} = sL_s + \frac{1}{sC_{gs}} + \frac{g_m L_s}{C_{gs}} = sL_s + \frac{1}{sC_{gs}} + \omega_T L_s \qquad (2.20)$$

As can be seen from (2.20), the source degeneration generates the

real part at the input impedance. This is important because there is no real part in Z_{in} without degeneration, while there is in Z_{opt}. Therefore, if not excessive, L_s helps to reduce the discrepancy between the real parts of Z_{opt} and Z_{in} of the LNA. Furthermore, from (2.20), the imaginary part of Z_{in} is changed by sL_s, and this is followed by the same change in Z_{opt}, as shown in (2.17).

For the circuit shown in Fig. 2.8(a), the condition that allows the SNIM is

$$Z_{opt} = Z_{in}^* \tag{2.21}$$

From (2.16)-(2.18) and (2.20), the conditions that satisfy (2.21) and matching with the source impedance Z_s are as follows:

$$Re[Z_{opt}] = Re[Z_s] \tag{2.22}$$
$$Im[Z_{opt}] = Im[Z_s] \tag{2.23}$$
$$Im[Z_{in}] = -Im[Z_s] \tag{2.24}$$
$$Re[Z_{in}] = Re[Z_s] \tag{2.25}$$

As described above, based on (2.20), (2.23) and (2.24) are the same, especially in advanced technology. Therefore, (2.24) should be dropped considering the importance of the noise performance. Some amount of mismatch in the input matching has a negligible effect on the LNA performance, while the mismatch in Z_{opt} directly affects the NF. Now then, from (2.16)-(2.20), the design parameters that can satisfy (2.22), (2.23) and (2.25) are V_{GS}, the transistor size W (or C_{gs}), and L_s. Minimum gate length is assumed to maximize the transistor cutoff frequency ω_T. Therefore, for the given value of Z_s, (2.22), (2.23) and (2.25) can be solved since three effective equations are provided with three unknowns.

The above LNA design technique suggests that, by the addition of L_s, in principle, the SNIM can be achieved at any values of Z_s by satisfying (2.22), (2.23) and (2.25) assuming (2.16)-(2.20) are valid. Many cases, especially those with large transistor size, high power dissipation, and high frequency of operation can be satisfied without much difficulty, while (2.16)-(2.20) stay valid. The problem occurs when

the transistor size is small (hence, the power dissipation is small) and the LNA operates at low frequencies. Equation (2.19) indicates that the small transistor size and/or low frequency leads to high value of **Re[Z_{opt}].** Therefore, from (2.20), for the given bias point or ω_T, the degeneration inductor L_s has to be very large to satisfy (2.25). The problem is that for the L_s to be greater than some value, (2.18) becomes invalid and F_{min} increases significantly. As a result, the minimum achievable NF of the LNA can be considerably higher than F_{min} of the common-source transistor, spoiling the idea of SNIM. In other words, the SNIM technique is not applicable for the transistor sizes and bias levels as **Re[Z_{opt}]** becomes greater than **Re[Z_{in}]** for the value of L_s, which does not degrade the F_{min} of the LNA. The inaccuracy of (2.18) for large L_s might be caused by the negligence of C_{gd}. With large L_s, the transconductance of the common-source stage can degrade significantly and the feedback signal through C_{gd} could become nonnegligible. As a practical design technique, the minimum value of L_s, which does not degrade F_{min}, can be identified by monitoring the F_{min} of the LNA as a function of L_s in simulation.
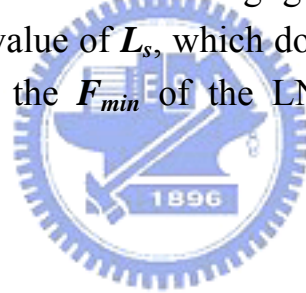
2.2.3 Power-Constrained Simultaneous Noise and Input Matching Technique

As described above, SNIM technique is not allowed at low-power implementations. However, the need for low-power implementation of a radio transceiver is one of the inevitable technical trends. Fig. 2.9(a) shows a cascoded amplifier topology that can satisfy the SNIM at low power. Note that the difference in Fig. 2.9(a) compared to the LNA shown in Fig. 2.8(a) is one additional capacitor C_{ex}. Fig. 2.9(b) shows the simplified small-signal equivalent circuit of Fig. 2.9(a). Again, in Fig. 2.9(b), the same simplifications are applied as in Fig. 2.7(b) and 2.8(b). The noise parameter equations can be derived by replacing (2.8) with the following expression:

$$\overline{i_{ng}^2} = 4kT\delta_{eff}\frac{\omega^2 C_t^2}{5g_{d0}}\Delta f$$

Where $\delta_{eff} = \delta(C_{gs}^2/C_t^2)$ and $C_t = C_{gs} + C_{ex}$. Equation (2.26) is the same expression as (2.8), but is just rewritten for simpler mathematics. The noise parameters can be given by

$$R_n = \frac{\gamma}{\alpha}\frac{1}{g_m} \tag{2.27}$$

$$Z_{opt} = \frac{\alpha\sqrt{\frac{\delta}{5\gamma(1-|c|^2)}} + j\left(\frac{C_t}{C_{gs}} + \alpha|c|\sqrt{\frac{\delta}{5\gamma}}\right)}{\omega C_{gs}\left\{\frac{\alpha^2\delta}{5\gamma(1-|c|^2)} + \left(\frac{C_t}{C_{gs}} + \alpha|c|\sqrt{\frac{\delta}{5\gamma}}\right)^2\right\}} - sL_s \tag{2.28}$$

$$F_{min} = 1 + \frac{2}{\sqrt{5}}\frac{\omega}{\omega_T}\sqrt{\gamma\delta(1-|c|^2)} \tag{2.29}$$
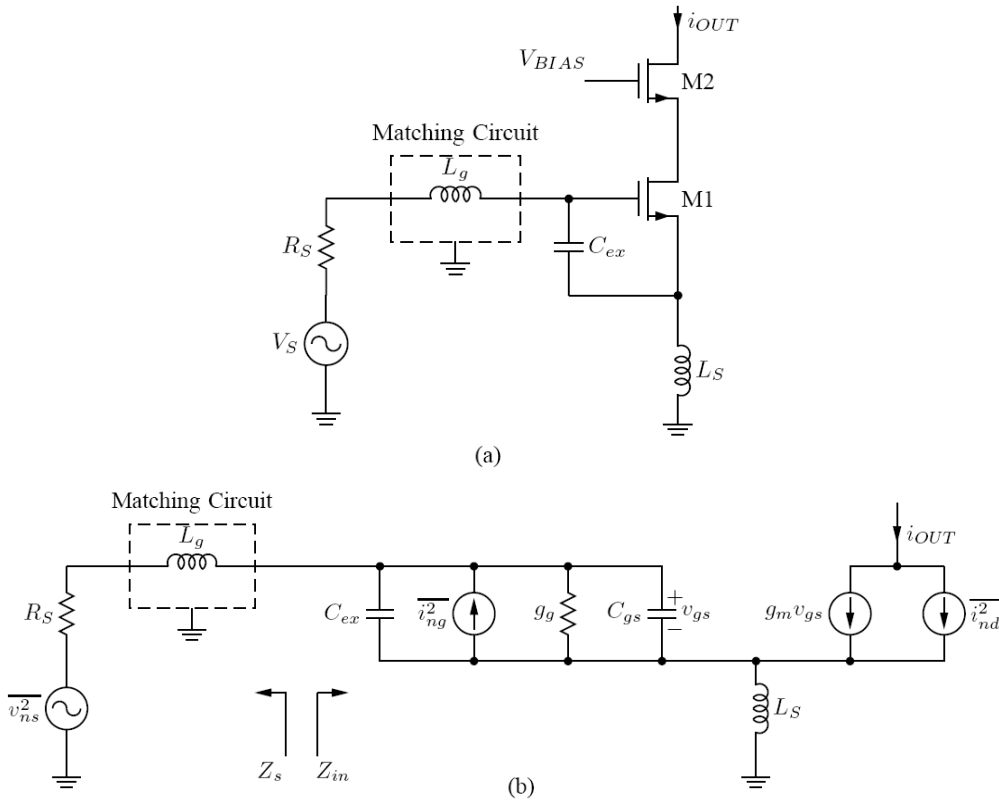
Fig. 2.9 (a) Schematic of a cascode LNA topology adopted to apply the PCSNIM technique. (b) Its small-signal equivalent circuit.

Interestingly, as can be seen from (2.27) and (2.29), the noise resistance R_n and minimum NF, F_{min}, are not affected by the addition of

C_{ex}, which is the same as the cases shown in Fig. 2.7 and Fig. 2.8. From Fig. 2.9(b), the input impedance of the LNA can be given by

$$Z_{in} = sL_s + \frac{1}{sC_t} + \frac{g_m L_s}{C_t} \qquad (2.30)$$

It can now be seen that the (2.27)-(2.30) are similar to (2.16)-(2.18) and (2.20). As discussed in Section 2.2.2, (2.27)-(2.29) are valid for rather small values of L_s.

As with the LNA topology shown in Fig. 2.8(a), for the SNIM of the circuit shown in Fig. 2.9(a), (2.21) now needs to be satisfied, and that means that the conditions shown in (2.22)-(2.25) should be satisfied. From (2.28) and (2.30), (2.22)-(2.25) can be re-expressed as follows:

$$\frac{\alpha\sqrt{\frac{\delta}{5\gamma(1-|c|^2)}}}{\omega C_{gs}\left\{\frac{\alpha^2\delta}{5\gamma(1-|c|^2)} + \left(\frac{C_t}{C_{gs}} + \alpha|c|\sqrt{\frac{\delta}{5\gamma}}\right)^2\right\}} = Re[Z_s] \qquad (2.31)$$

$$\frac{j\left(\frac{C_t}{C_{gs}} + \alpha|c|\sqrt{\frac{\delta}{5\gamma}}\right)}{\omega C_{gs}\left\{\frac{\alpha^2\delta}{5\gamma(1-|c|^2)} + \left(\frac{C_t}{C_{gs}} + \alpha|c|\sqrt{\frac{\delta}{5\gamma}}\right)^2\right\}} - sL_s = Im[Z_s] \qquad (2.32)$$

$$sL_s + \frac{1}{sC_t} = -Im[Z_s] \qquad (2.33)$$

$$\frac{g_m L_s}{C_t} = Re[Z_s] \qquad (2.34)$$

As discussed in Section 2.2.2, for the typical values of advanced CMOS technology parameters, (2.32) is approximately equal to (2.33). Therefore, (2.33) can be dropped, which means that, as in Section 2.2.2, for the given value of L_s, the imaginary value of the optimum noise impedance becomes approximately equal to that of the input impedance with an opposite sign $Im[Z_{in}] \approx -Im[Z_s]$ automatically. The design parameters that can satisfy (2.31), (2.32) and (2.34) are V_{GS}, W (or C_{gs}), L_s, and C_{ex}. Since there are three equations and four unknowns, (2.31), (2.32) and (2.34) can be solved for an arbitrary value of Z_s by fixing the value of one of the design parameters. Therefore, in the PCSNIM LNA design technique, by the addition of an extra capacitor C_{ex}, the SNIM can

be achieved at any level of power dissipation.

Note that, like the case of the SNIM technique, (2.27)-(2.29) are derived assuming L_s is not very large. The validity of this assumption in a low-power LNA can be investigated. From (2.31) and (2.34), the following approximated relation can be made:

$$L_s \approx \frac{\alpha \sqrt{\frac{\delta}{5\gamma(1-|c|^2)}}}{\omega \omega_T C_t} \qquad (2.35)$$

Equation (2.35) indicates that L_s is a function of C_t and ω_T (which is a function of V_{GS}). In comparison, for the SNIM technique, a similar relation can be obtained from (2.17), (2.22) and (2.25) as

$$L_s \approx \frac{\alpha \sqrt{\frac{\delta}{5\gamma(1-|c|^2)}}}{\omega \omega_T C_{gs}} \qquad (2.36)$$

By comparing (2.35) and (2.36), it can be seen that, in the PCSNIM technique applied for the low-power design, where C_{gs} is small, the required degeneration inductance L_s can be reduced by the addition of C_{ex}. In fact, by applying the PCSNIM technique to the SNIM technique-based LNA, the required degeneration inductance L_s can be reduced below what the SNIM technique requires.

2.3 The Principal Concepts of Mixer

Mixers are responsible for frequency translation by multiplying two signals (and possibly their harmonics). They employed in the receive path have two distinctly different inputs, called the RF port and the LO port. The RF port senses the signal to be downconverted or upconverted and the LO port senses the periodic waveform generated by the local oscillator.

There are many ways to implement a mixer. The simplest idea is to have the LO signal turn on and off the switch in the RF path as shown in Fig. 2.10(a). In integrated circuit, an ideal switch is always implemented by a NMOS as shown in Fig. 2.10(b). For simple switch mixer, the waveform for the LO can be modeled as a return-to-zero (RTZ) square waveform. The mixer output can be modeled as

$$V_o(t) = V_{RF}\cos(\omega_{RF}t) \cdot \left[\frac{1}{2} + \sum_{n=1}^{\infty} \frac{\sin(n\frac{\pi}{2})}{n\frac{\pi}{2}}(\cos(n\omega_{LO}t))\right] \qquad (2.37)$$

(a)

(b)
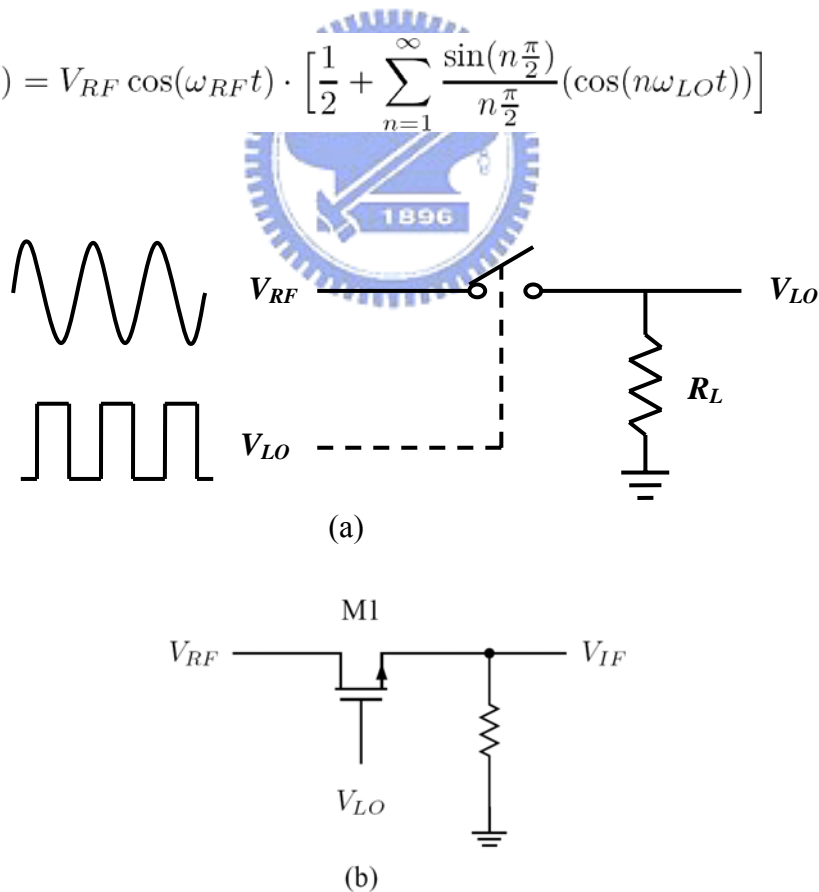
Fig. 2.10   (a)Simple switch used as mixer, (b)implementation of switch with an NMOS device

From (2.37), it is obvious that RF component will be duplicated at upper sideband and lower sideband around LO and its odd harmonics. The upper sideband or lower sideband around LO are so-called IF components. It depends that the mixer is downconversion or upconversion. The sidebands around LO's harmonics are not desired. Usually, they must be suppressed by filter [24] or mixer itself. The DC term in the bracket means that the RF signal is not suppressed.

2.3.1 Typical Mixer

Fig. 2.11 indicates standard single-balanced mixer. M3 is an RF buffer amplifier, while M1 and M2 provide the switching function needed for mixing action. Since M1 and M2 are not on at the same time, the output mixed signal is single ended
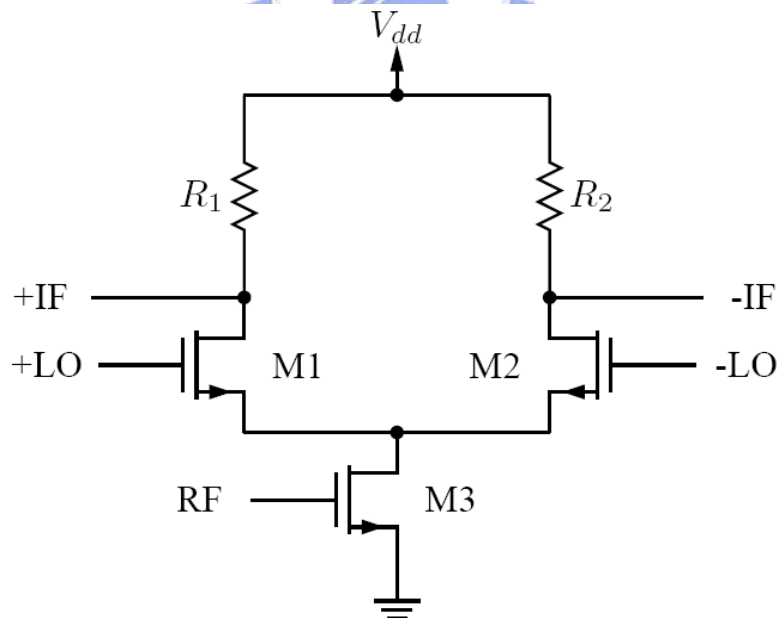
Fig. 2.11   Standard single-balanced mixer.

Fig. 2.12 indicates standard double-balanced mixer. The LO simply changes/modulates the phase of the RF signal between 0° and 180°. The output is never grounded. The mixing result is modeled by

$$V_o(t) = 2V_{RF}\cos(\omega_{RF}t) \cdot \left[\sum_{n=1}^{\infty} \frac{\sin(n\frac{\pi}{2})}{n\frac{\pi}{2}}(\cos(n\omega_{LO}t)) \right] \qquad (2.38)$$

Above equation states that, in theory, by using the NRTZ switching waveform, the DC term in the equation is completely eliminated. Thus, the RF signal is greatly suppressed
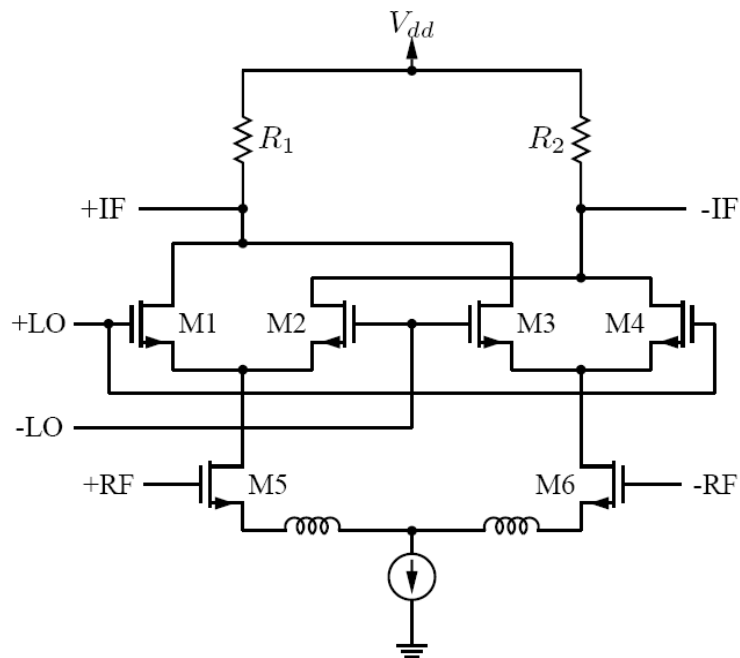
Fig. 2.12   Standard double-balanced mixer.
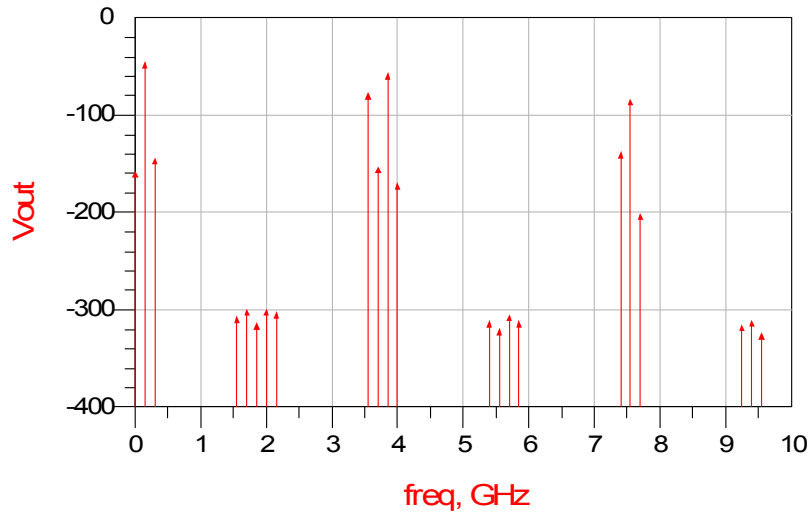
Fig. 2.13   The Simulated Result of Standard double-balanced mixer.

2.3.2   Sub-harmonic Mixer

There are three approaches to design sub-harmonic mixer. The first approach is based on a basic trigonometric equation

$$\sin(2\omega) = 2\sin(\omega)\cos(\omega) \qquad (2.39)$$

Above equation basically shows that, if the LO signal is phase-shifted by 90° and then multiplied by the original LO, twice the frequency of the LO is produced. This is exactly the property needed in a SHM. It is easily implemented by stacking another switching stage in the mixer. The non-balanced and single-balanced implementations of such a SHM are shown in Fig. 2.14 and Fig. 2.15. For the non-balanced SHM, an RC network is used to create the 90° phase shift. It is then used to drive the two switching stages of the mixer. For the single-balanced SHM, a polyphase network is used to generate the 0° and 180°, 90° and 270° signal pairs. The double-balanced version is obtained by simply cross coupling two single-balanced SHMs.
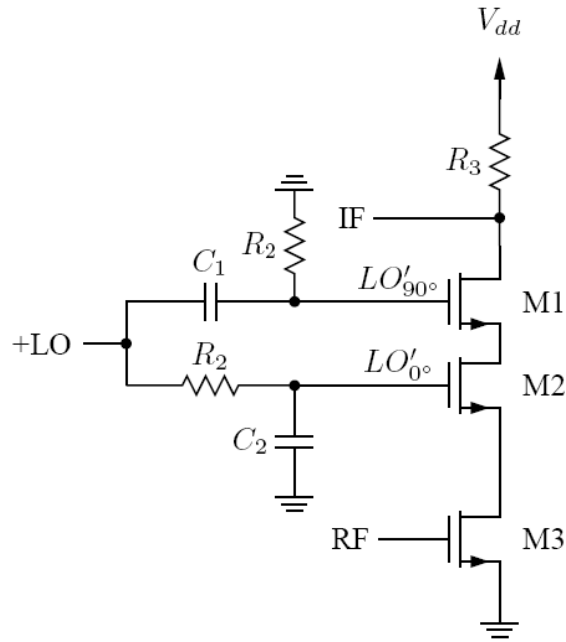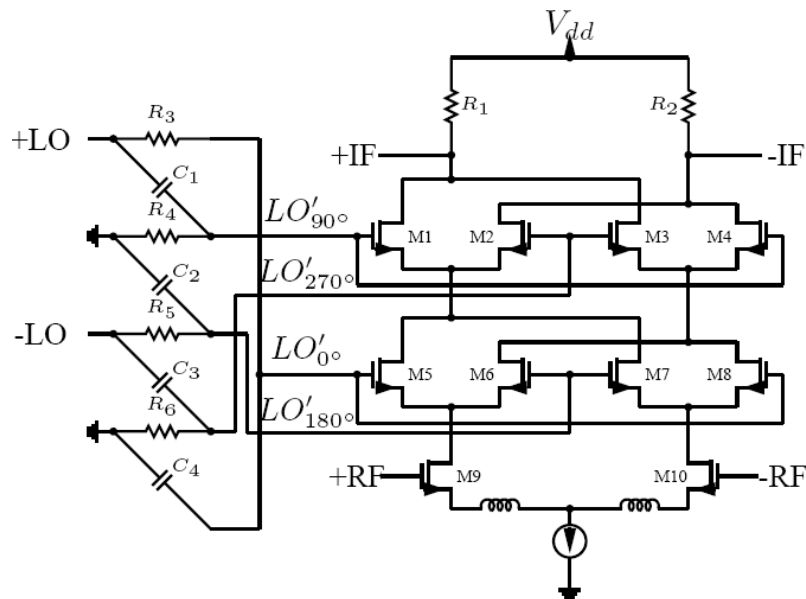
Fig. 2.14　Single-ended stacked sub-harmonic mixer.

Fig. 2.15　Single-balanced stacked sub-harmonic mixer.

The second generalized approach is based on yet another simple equation
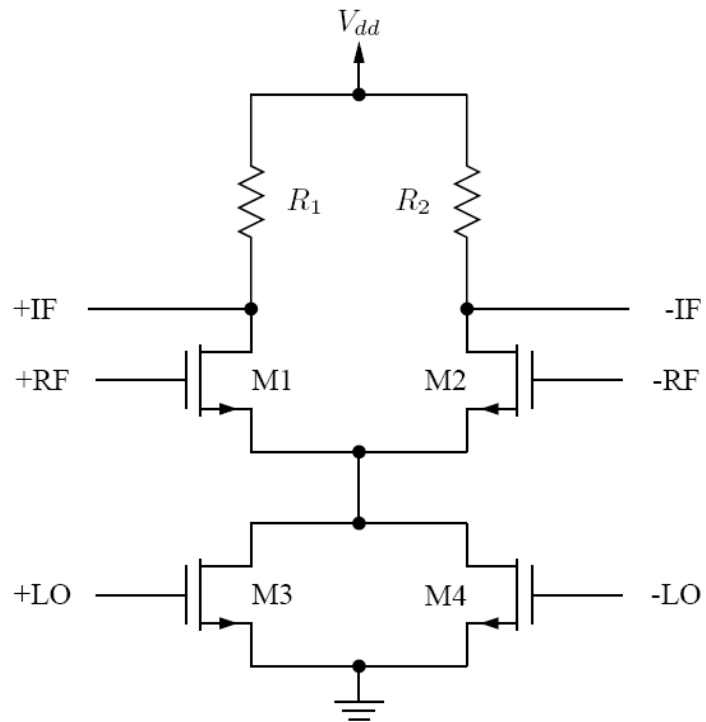
$$f(x) = |x| \qquad (2.40)$$
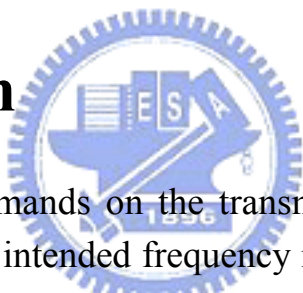
Fig. 2.16   Single-balanced sub-harmonic mixer.

Chapter 3
The Implementation of 4GHz to 20GHz Designing Low Noise Amplifier and Mixer

A 4HGz to 20GHz wide-band low noise amplifier is designed in Simultaneous Noise and Input Matching Technique, and fabricated in TSMC 0.18μm CMOS technology.

3.1 Induction

With much more demands on the transmission of data, voice, and video, it is urgent that the intended frequency range for the LNA needs to become wider. However, most published papers only specify the mechanism of one-pole matching for LNA. One-pole matching is difficult to achieve wide-band matching.

In this project, we would like to design an ultra-wide band low noise amplifier, which is implemented based on UMC 0.18 um CMOS technology. The frequency range of operation is from 4 to 20 GHz, and under this range the input reflection coefficient must be under -10 dB and power gain must be large than 20 dB. This design utilizes common SNIM technique, which can simultaneously achieve noise and input matching. Besides, capacitor feedback technique is also applied in the design for realizing ultra-wide band requirement.

3.2 Principle of Circuit Design

This project is achieved on Angilent ADS. Fig. 3.1 is the input stage of wide-band low noise amplifier. Transmission lines, TL22 and TL23, are utilized to emulate the effects of inductors. Each μm transmission line has around the effect of around 1pH inductance. Basically, the structure is utilized the SNIM technique plus capacitor parallel-feedback technique. While the circuit operates at high-frequency, C20 can be considered as short circuit. The input impedance of the circuit consists of C20、T23、T24、R1 and the input impedance of next stage, and the 50Ω input impedance can be achieved.
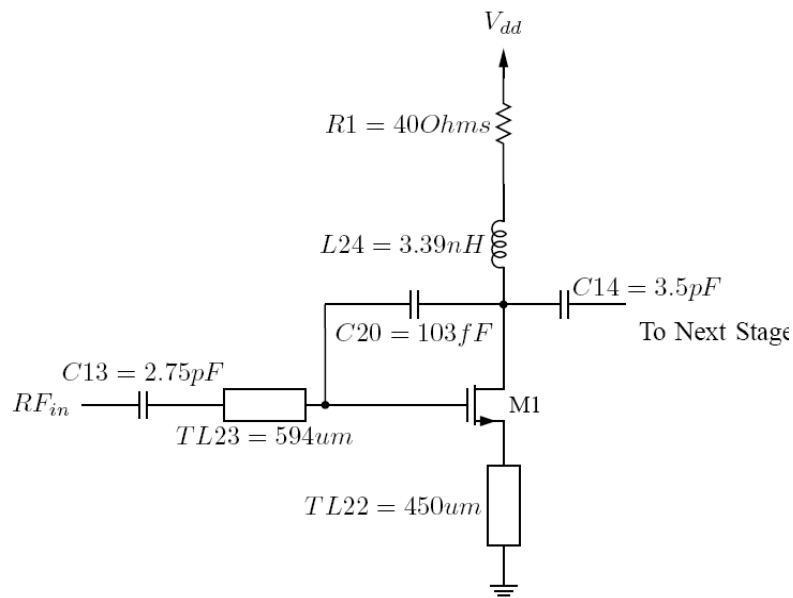
Fig. 3.1　The input stage of wide-band low noise amplifier.

While the circuit operates at high-frequency, owing to millier effect on C20, there is an equivalent capacitor at the gate of transistor M1. It parallel with the input capacitor of M1 C_{gs}, and make input match at lower frequency. Though resistors will increase noise figure, R1 doesn't contribute noise much. That is because it is located at the output of first stage, and the gain of first stage is not very lower. Besides, R1 is essential for increasing the stability of circuit.
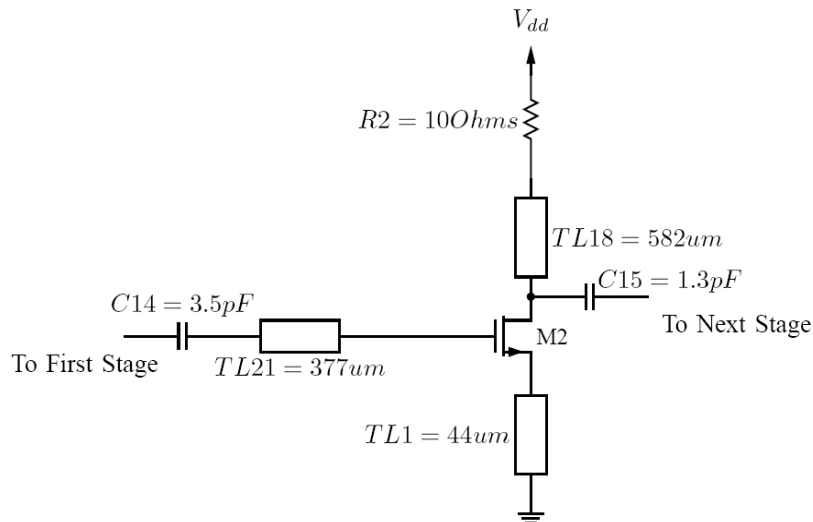
Fig. 3.2　The second stage of wide-band low noise amplifier.

Fig. 3.2 is the second stage of this project. Again, it is also a common-mode source amplifier. Its gain is around 10dB.
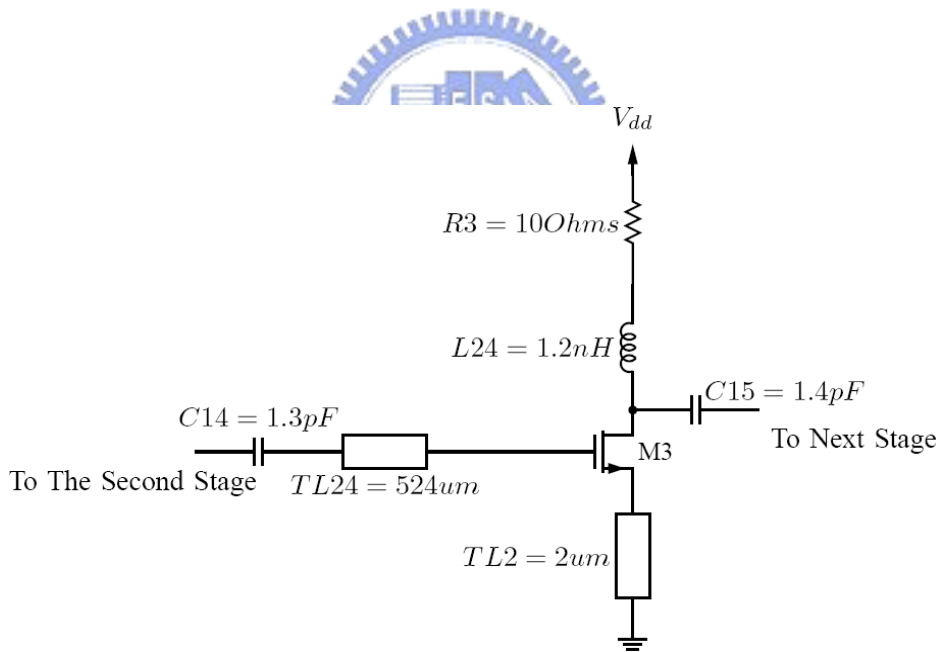

Fig. 3.3　The third stage of wide-band low noise amplifier.

Fig. 3.3 is the third stage of this project. Again, it is also a common-mode source amplifier, too. Its gain is also around 10dB.
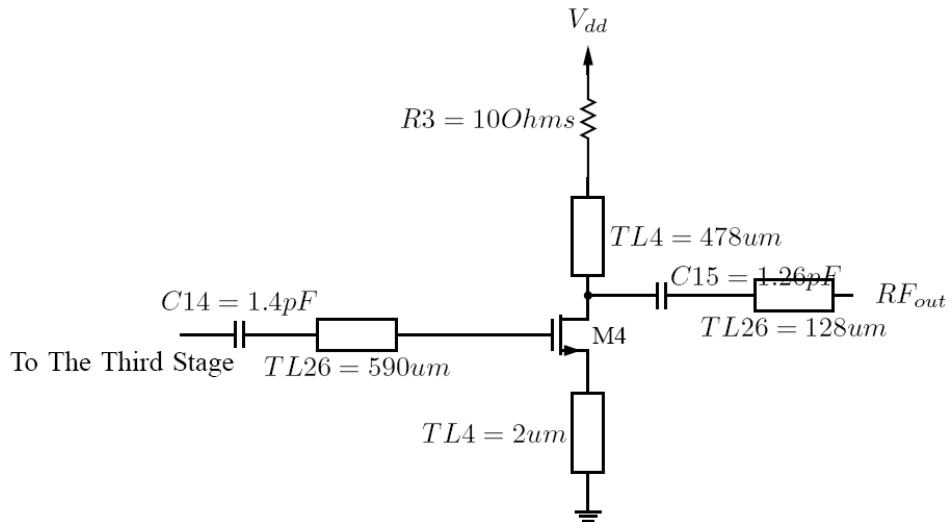
Fig. 3.4   The last stage of wide-band low noise amplifier.

Fig. 3.4 is the last stage of this project. Similarly, it is also a common-mode source amplifier. Its gain is also around 5dB. The output impedance matching is achieved by LC networks.
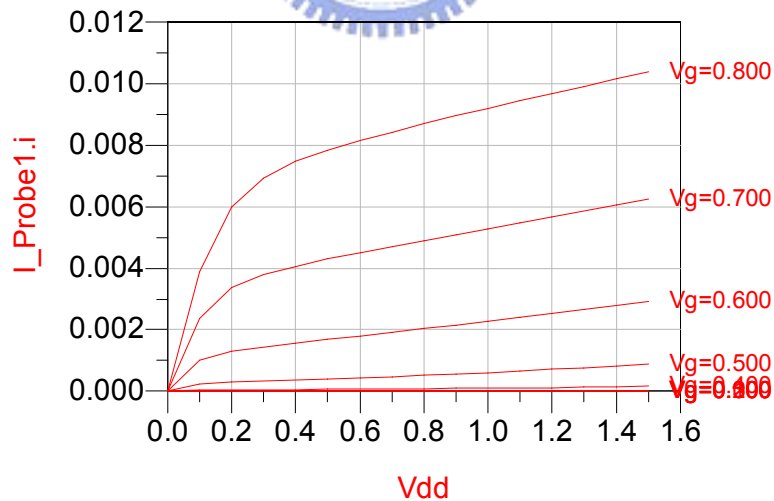
3.3   The Simulated Results

Fig. 3.5   The simulated DC characters of single transistor

Fig. 3.5 are the simulated DC characters of single transistor, while V_g is 0.8V voltages, V_{dd} is 1.5V voltage, and I_{d1} is around 10.5mA

Fig. 3.6   The simulated S-parameters of wide-band low noise amplifier

freq (100.0MHz to 40.00GHz)

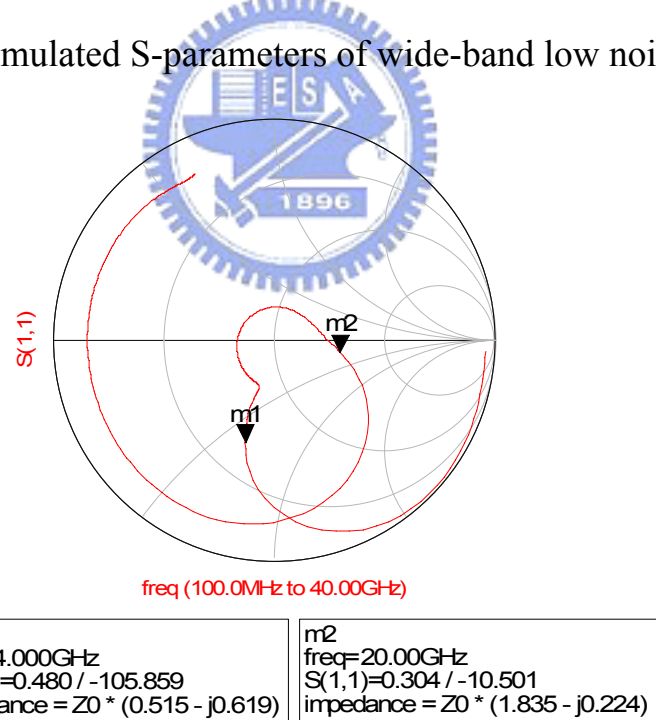| m1	m2
freq=4.000GHz	freq=20.00GHz
S(1,1)=0.480 / -105.859	S(1,1)=0.304 / -10.501
impedance = Z0 * (0.515 - j0.619)	impedance = Z0 * (1.835 - j0.224)

Fig. 3.7   The simulated input reflection coefficient (S_{11}) on Smith chart
of wide-band low noise amplifier

Fig. 3.6 and Fig. 3.7 are the simulated results on Angilent ADS. The power gain on intended frequency range is up to 22dB, reflection coefficient at input terminal is lower than -10dB, and the noise

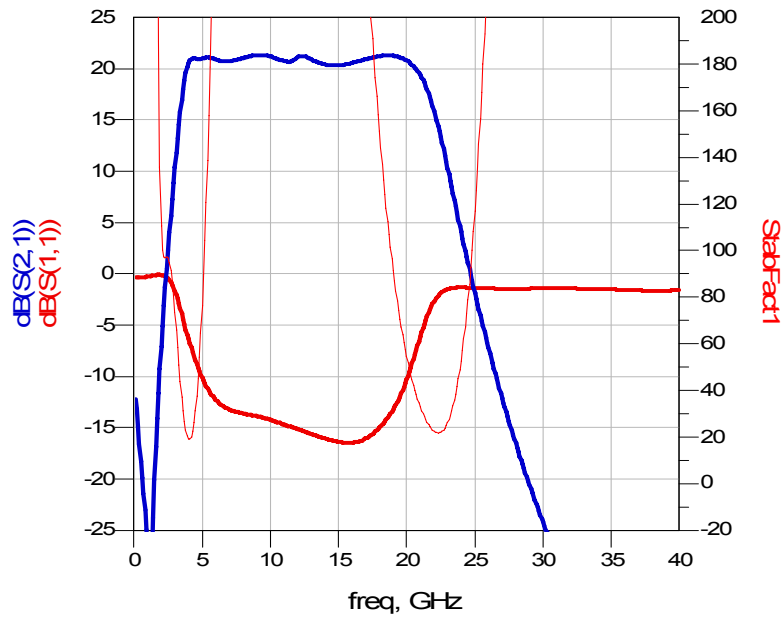temperature is lower than 600 degrees centigrade.

Fig. 3.8   The simulated stability factor of wide-band low noise amplifier

Fig. 3.8 is the simulated stability factor. Obviously, the circuit is stable on intended frequency range.

3.4 Expected Specifications

Parameters	Values
Bandwidth	4-20GHz
S_{21} [dB]	21-22
Noise Temperature[K]	Under 300
S_{11}[dB]	under -10
Power dissipation[mw]	50.4
Technology[um]	0.18

Table. 3-1 The expected specifications of wide-band low noise amplifier

Power consumption is estimated while LNA operates at DC. Each transistor consumes 7mA current. Four transistors consume 50.4mW power when power supply is 1.8V.
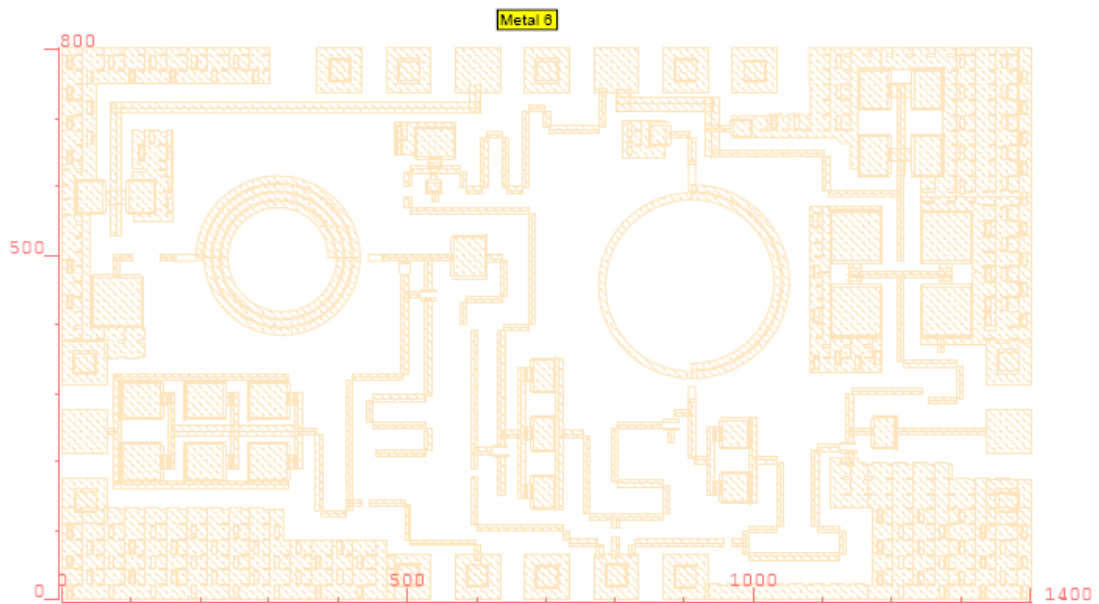
3.5   The Layout of Wide-Band LNA

Fig. 3.9   The metal 6 of wide-band low noise amplifier layout
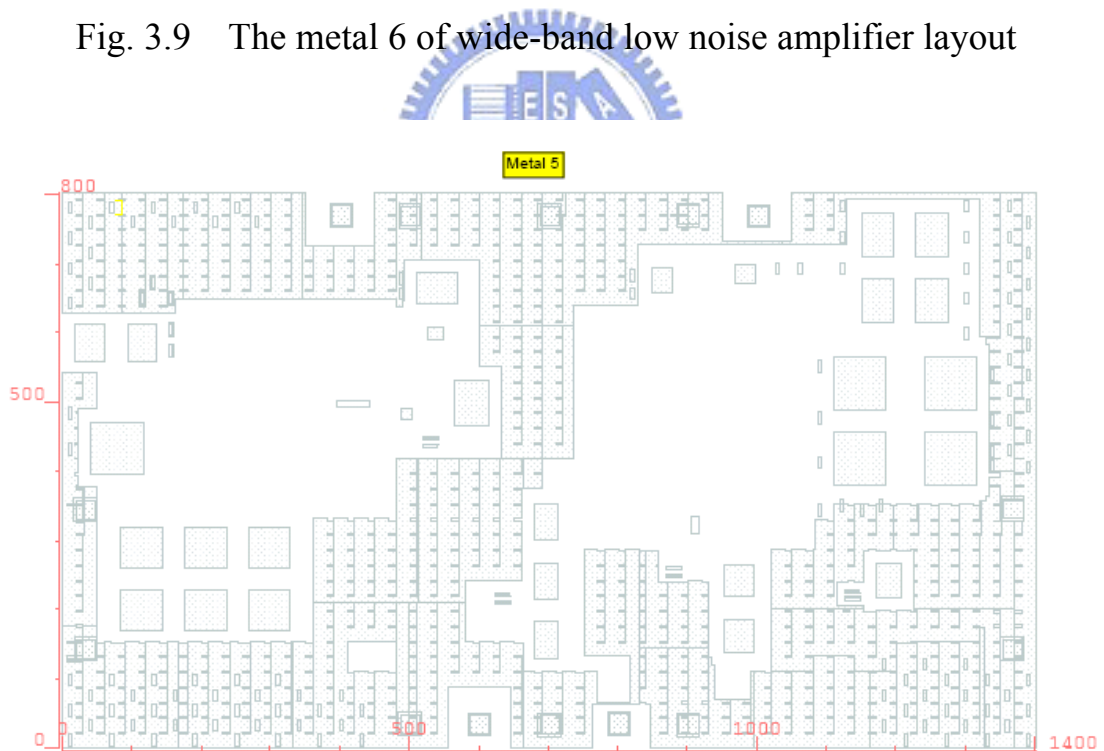

Fig. 3.10   The metal 5 of wide-band low noise amplifier layout
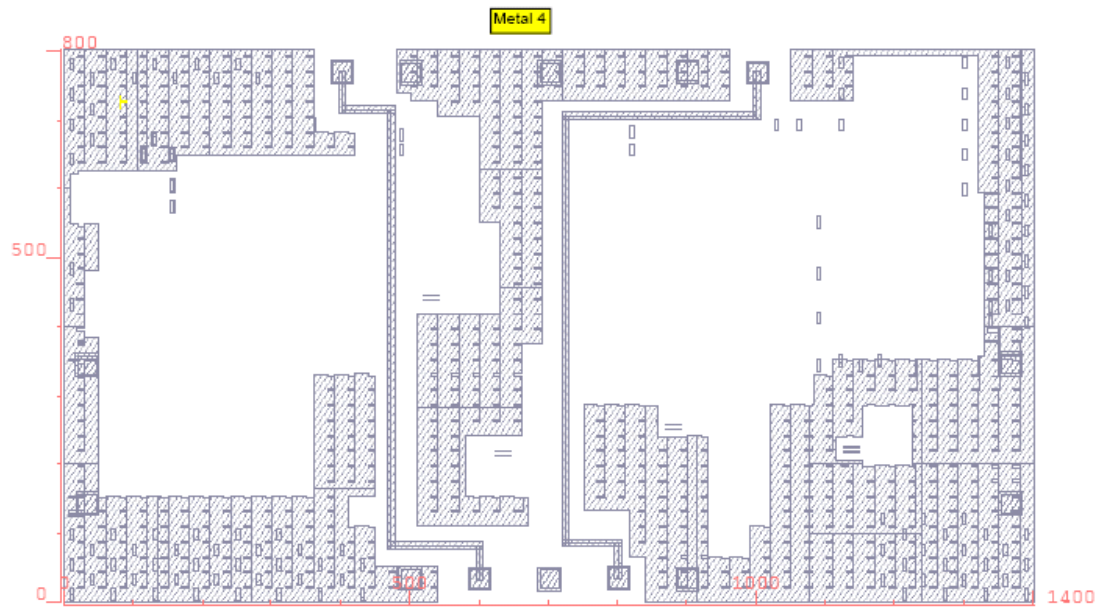
Fig. 3.11   The metal 4 of wide-band low noise amplifier layout
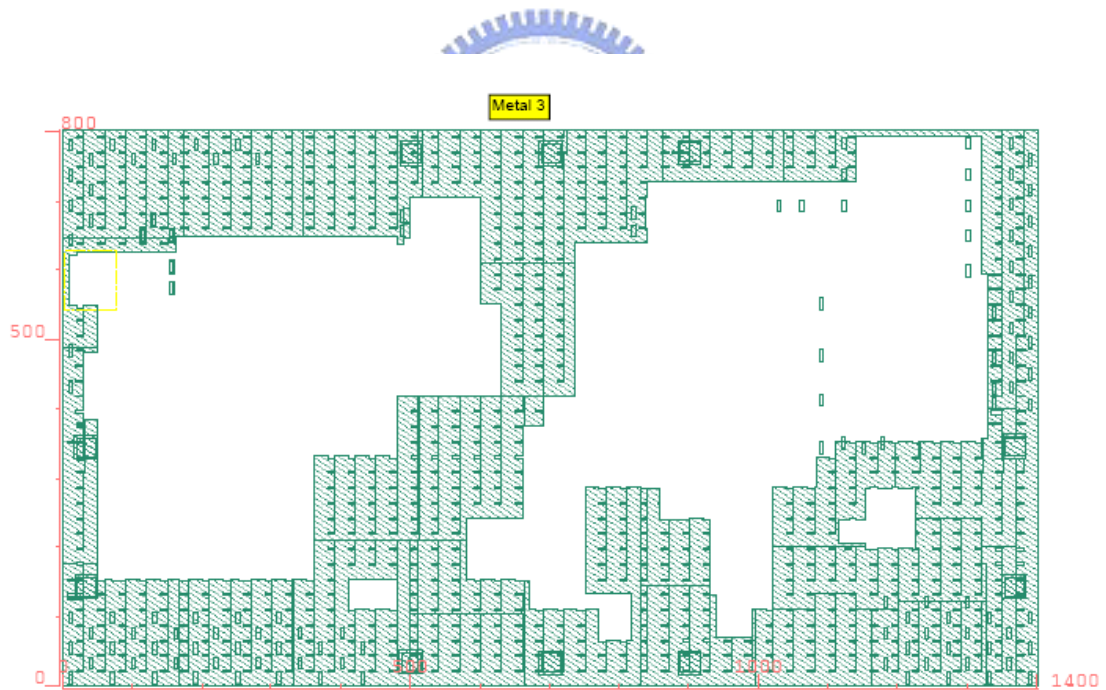

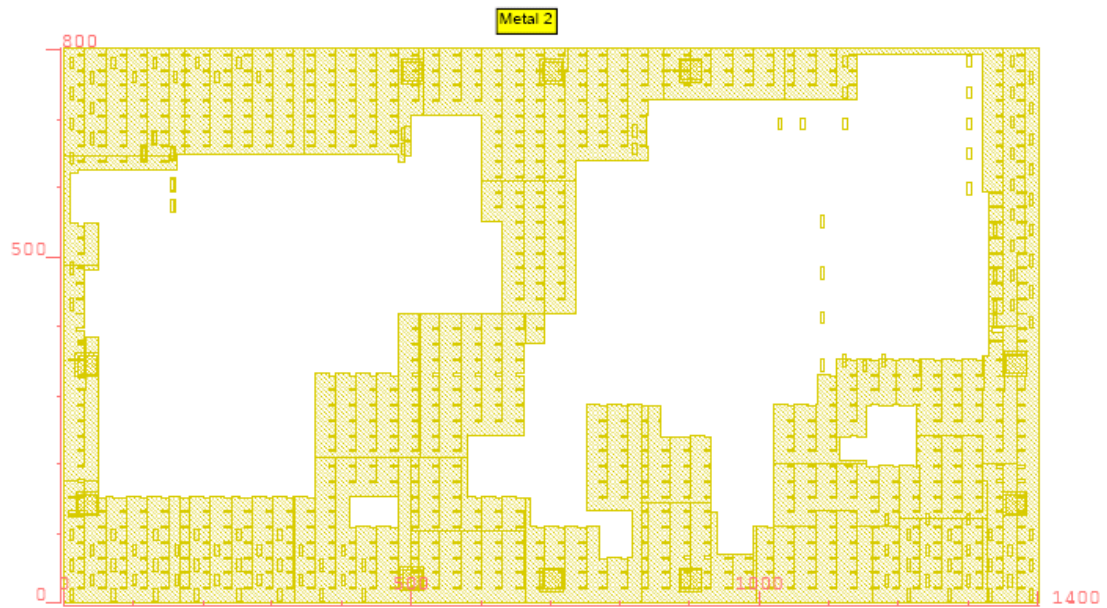Fig. 3.12   The metal 3 of wide-band low noise amplifier layout

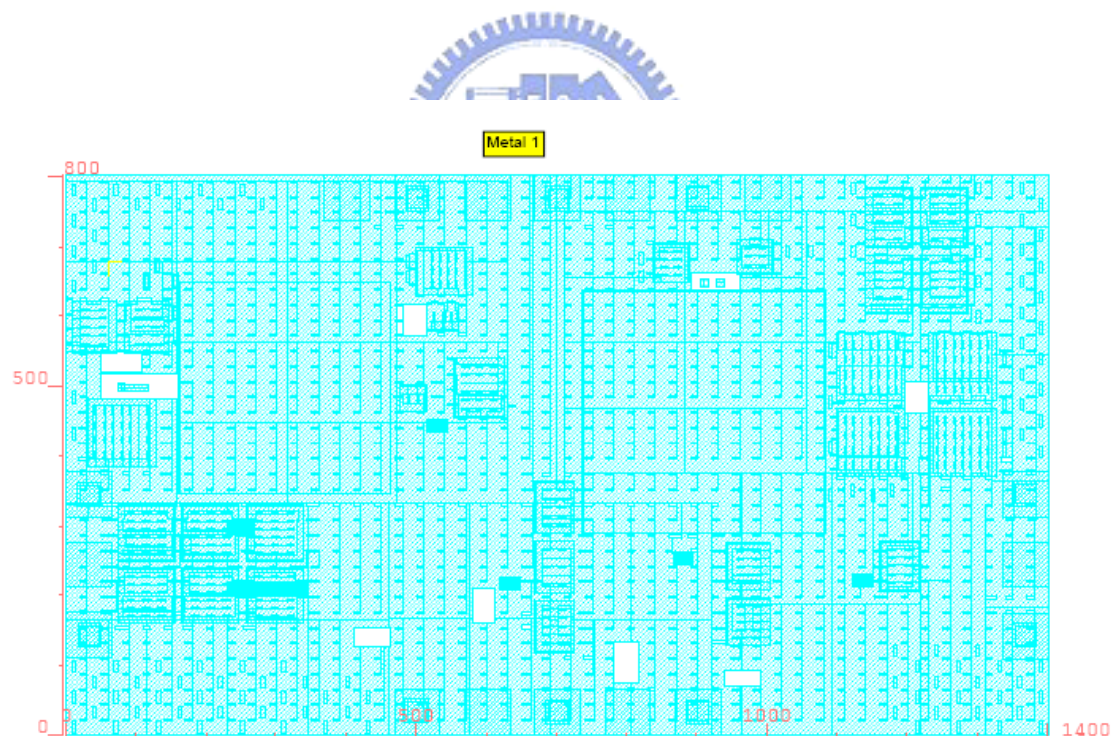Fig. 3.13   The metal 2 of wide-band low noise amplifier layout

Fig. 3.14   The metal 1 of wide-band low noise amplifier layout

Fig. 3.9 to Fig. 3.14 are the layout of wide-band low noise amplifier, have the dimension 1400 x 800 x 1200 μm and are fabricated by TSMC 0.18μm technology.

3.6   Measurement

difficult to set a probe here
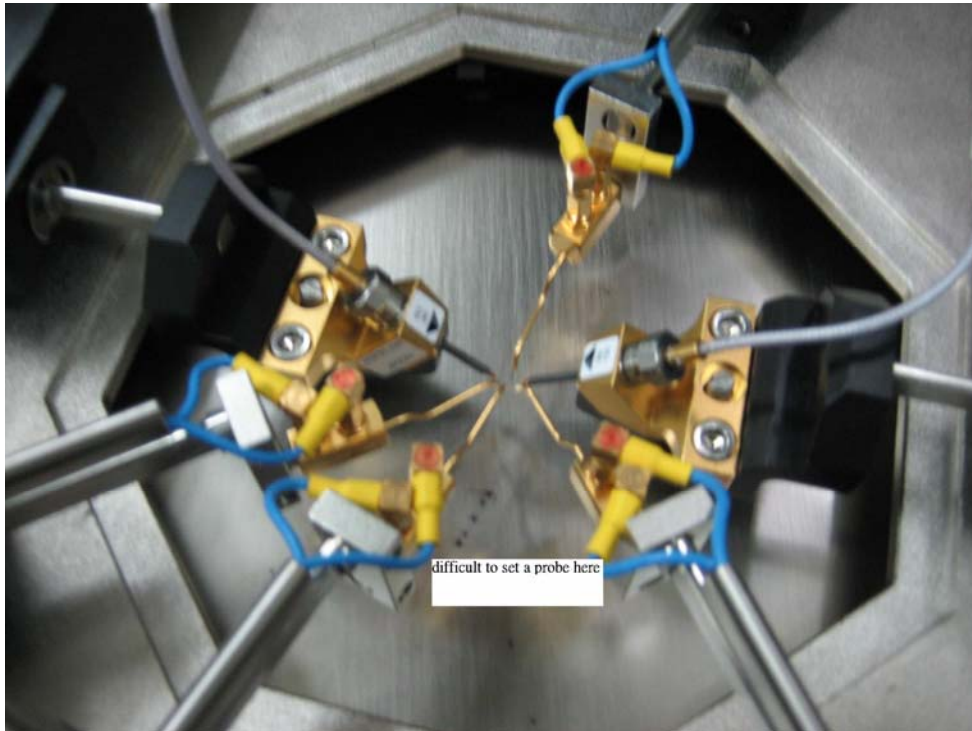
Fig. 3.15   The testing environment at VIA RF lab.

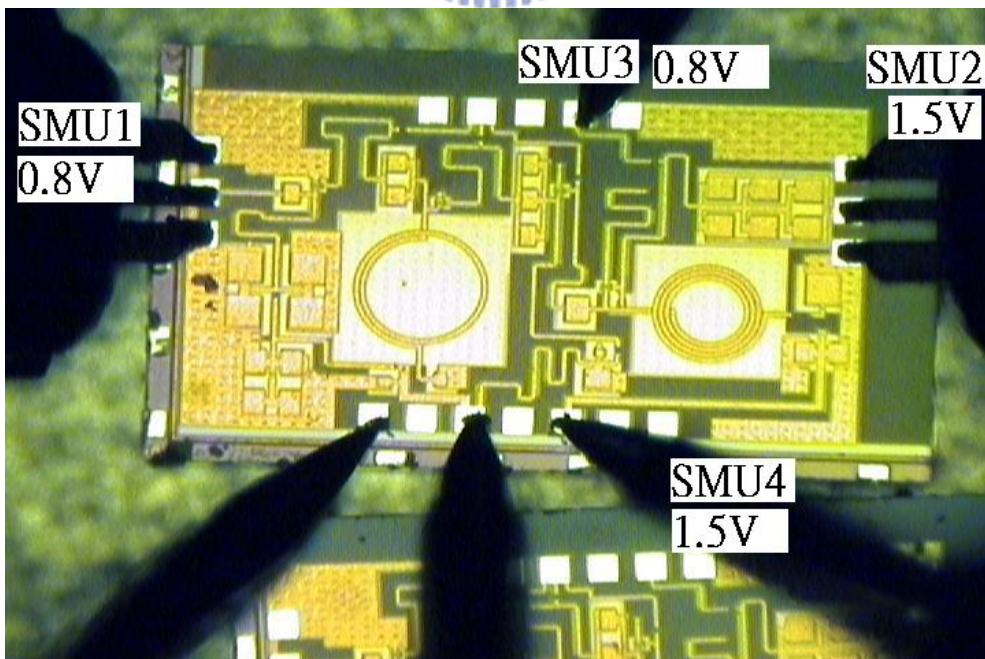SMU3 0.8V   SMU2 1.5V

SMU1 0.8V

SMU4 1.5V

Fig. 3.16   The testing probes and dice of wide-band LNA.

We measured the dice by IC-cap at VIA technology LTD. Fig. 3.15 indicates the testing environments. The effective testing frequency range of RF probes and testing instruments can be up to 50GHz. While measuring, two sets of RF probes are essential. One is for input terminal, and the other is for output terminal. Besides, four DC probes are necessary for DC feeding. They are fed into V_{gg1}、V_{gg2}、V_{dd1} and V_{dd2} respectively. V_{gg1} and V_{gg2} are fed by 0.8V voltages. V_{dd1} and V_{dd2} are fed by 1.5V voltages. The testing probes and dice of wide-band LNA is shown in Fig. 3.16. In order to measure the device accurately, we need to calibrate RF probe and testing instruments before measuring

3.7   Measurement Results

We first measured DC characters of the transistor on first stage. The measured is shown in Fig. 3.17. While V_{gg1} is 0.8V voltage, we could measure that I_{d1} is around 9mA. Compared with simulated results, the measured result is not out of our expectations.
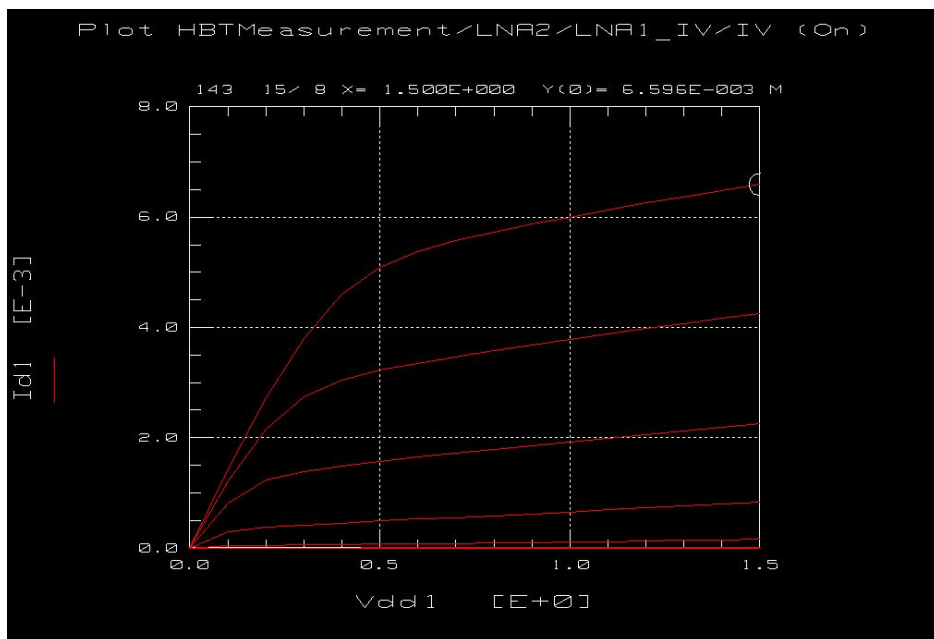

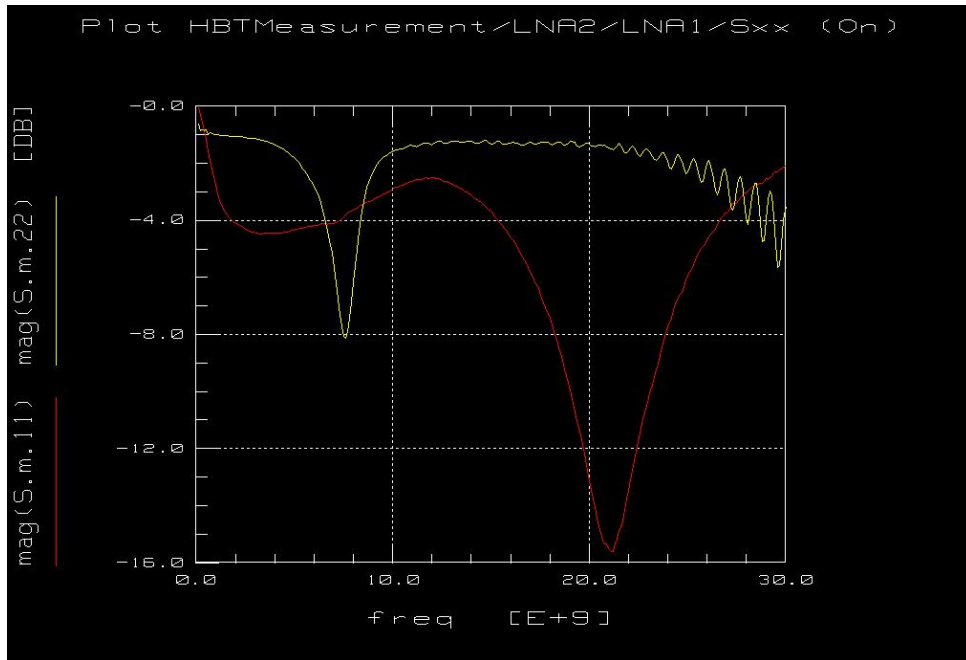Fig. 3.17   The measured DC characters of the transistor on first stage

Fig. 3.18   The measured input reflection coefficient (S_{11}) and output
reflection coefficient (S_{12})

The measured input reflection coefficient (S_{11}) and output reflection coefficient (S_{12}) are shown in Fig. 3.18. Due to the restriction of instruments, we fed the port 1 of instrument into the output of device and port 2 into the input of device. Therefore, the S_{11} on Fig. 3.18 actually is output reflection coefficient (S_{22}), and S_{22} is the input reflection coefficient (S_{11}). From Fig. 3.18, we found that the measured results are far from like the simulated results. S_{11} is not lower than -10dB in intended frequency range, and S_{22} is lower than -10dB from 19.5GHz to 21.5GHz.
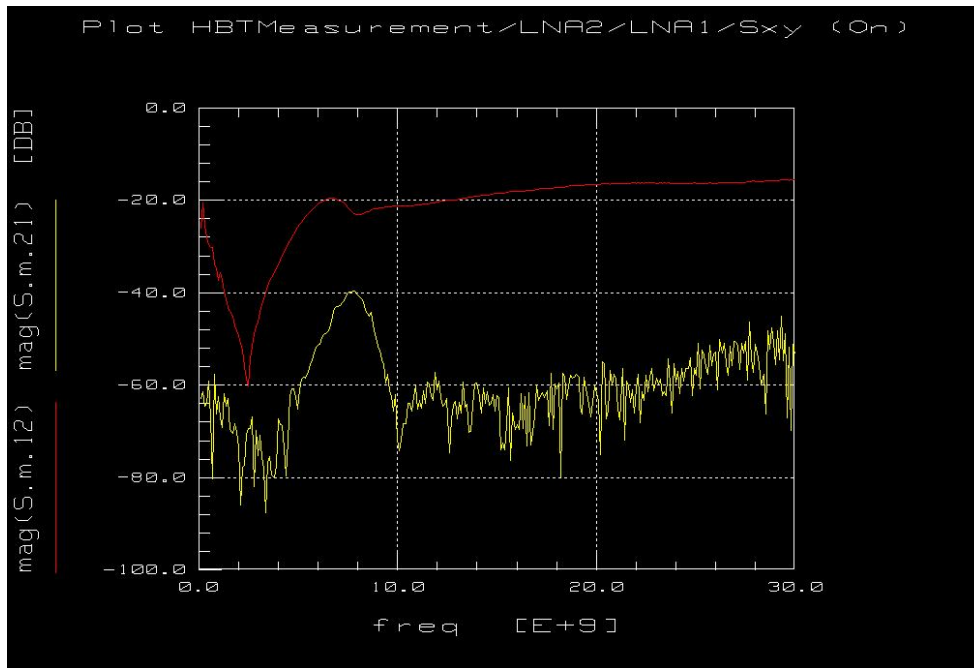
Fig. 3.19   The measured forward transmission coefficient (S_{21}) and
reverse transmission coefficient (S_{12})

The measured forward transmission coefficient (S_{21}) and reverse transmission coefficient (S_{12}) are shown in Fig. 3.19. Similarly, due to the restriction of instruments, we fed the port 1 of instrument into the output of device and port 2 into the input of device. Therefore, the S_{21} on Fig. 3.19 actually is reverse transmission coefficient (S_{12}), and S_{12} is the forward transmission coefficient (S_{21}). The measured forward transmission coefficient (S_{21}) is around -22dB to -16dB. Compared with simulated result, there are a lot of differences.

3.8   Conclusion For Wide-Band LNA

The chip malfunctions, and we have some ideas which might be the root causes.

A. The issues on layout

In this project most components are placed on metal 6, and metal 2 to metal 5 are placed on ground plane. Owing to there are 0.8μm gap

between metal 5 and metal 6, it will result in much effects of parasitic capacitor under many transmission lines which are utilized to imitate inductors. It makes the character of whole circuit greatly change. Therefore most places on metal 2 to metal 5 should be reserved.

B. The issues on the settings of ADS

While simulating on ADS, some parameters about substrate are not correctly set, such as the height of substrate. Owing to metal 5 is placed on ground plane, the correct height of substrate is 0.8μm. Besides, the dielectric constant is set wrong, too. Though, it won't greatly change input reflection coefficient, it will make power gain not to be so flat any more under intended frequency range. After changing wrong parameters to correct ones and simulating again, we found the simulated results are very like to measured results. The simulated results are shown Fig. 3.20.

C. The issues on components placement

In our design, we utilize many components provided by wafer company. The places under inductor, between metal 2 to metal 5, shouldn't be placed ground plane. It doesn't make the characters of components consist with the ones provided by wafer company. Besides, after completing simulation on ADS, it is essential to run Momentum to verify the characters of inductors and transmission lines. The works on running Momentum are omitted.
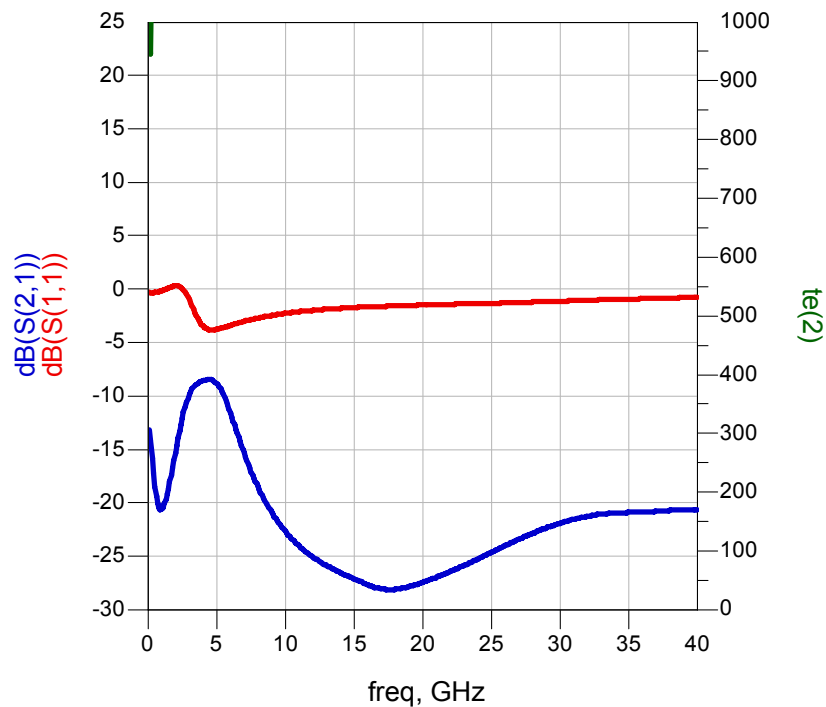
Fig. 3.20   The simulated input reflection coefficient (S_{11}) and output reflection coefficient (S_{12}) after changing wrong parameters to correct ones

D. The issues on transmission lines

The places under inductor, between metal 2 to metal 5, shouldn't be placed ground plane, and we should place ground place on right metal refer to the height of substrate. Besides, we should run Momentum to verify the characters of transmission lines.

E. We should consider testing environments before designing circuit

While designing circuit, we place two 300μm bond wires at input and output terminals. However, while measuring, there is no bond wire in the circuit. Though it won't change the character a lot, we should consider testing environments before designing circuit.

Chapter 4

The Design of Novel Mixer

4.1 Induction

The intermodulation performance of a receiver front end is often limited by that of the mixer. This is because the mixer performance is usually worse than that of the other stages, and the mixer must handle the largest signal levels. Consequently, in most low-noise capability can do much to improve dynamic range.

The most commonly used mixers in microwave systems employ Schottky-barrier diodes as the mixing elements. These are usually used in balanced structures to separate the RF and local oscillator (LO) signals, to improve large-signal capability, and to reject certain even-order spurious responses and intermodulation products. Because the Schottky diode is very strongly nonlinear, diode mixers have at best mediocre intermodulation susceptibility.

Nowadays the most popular used topology of mixer is Gilbert Cell. Many papers discussing Gilbert Cell are published on international journals. In the chapter, we propose a novel mixer which is never published in worldwide international papers.

4.2 Operating Principle

Mixers are conventionally realized by applying a large LO signal and a small RF signal to a nonlinear device, usually a Schottky-barrier diode. The LO modulates the junction conductance at the LO frequency, allowing frequency conversion. In principle, this conductance could be

realized via a time-varying linear conductance, rather than a nonlinear one, resulting in a mixer without intermodulation. A simple examples of such a time-varying linear element, which is capable of intermodulation-free mixing, is an ideal switch, operated at the LO frequency, in series with a small resistor.

Fig. 4.1 shows a conventional very low intermodulation mixer(VLIM). To realize a mixer, the MOS is operated in common-source configuration, the *LO* is applied to the gate, with proper DC bias, and the *RF* is applied to the drain. The *IF* is filtered from the drain. The relatively large value of C_{gd} would couple the *RF* and *LO* circuits to an unacceptable degree, so for a single-device mixer, *RF* and *LO* filters must be used. It is important that the *LO* voltage not be coupled to the drain terminal; if it is, the drain voltage will traverse the more strongly nonlinear portion of the *V/I* curve, increasing the IM level. The RF filter should therefore be designed to short-circuit the drain at the *LO* frequency. The design goal for the LO filter is not so clear. If *RF* voltage is coupled to the gate, it is conceivable that intermodulation could be increased because of the nonlinearities in G_m. If the gate is shorted at the *RF* frequency, no *RF* voltage appears on the gate, so there is no possibility of IM generation in this way. However, open-circuiting the gate effectively halves the capacitance in parallel with the channel resistance, so conversion loss should be lower. In the mixer described here, the *LO* filter was designed to short-circuit the *RF* at the gate.
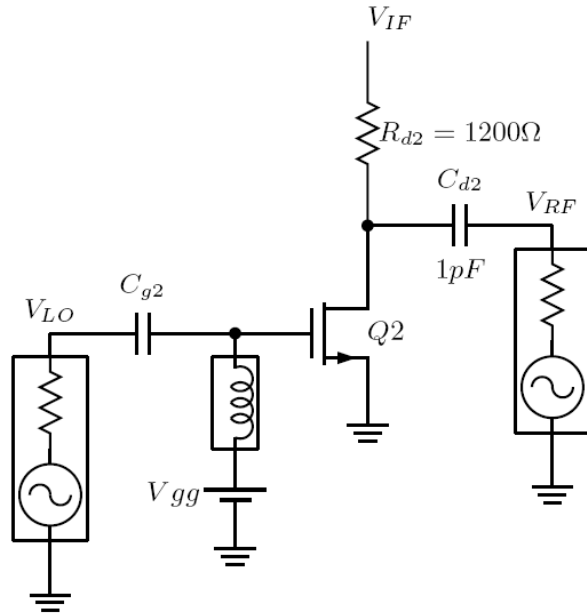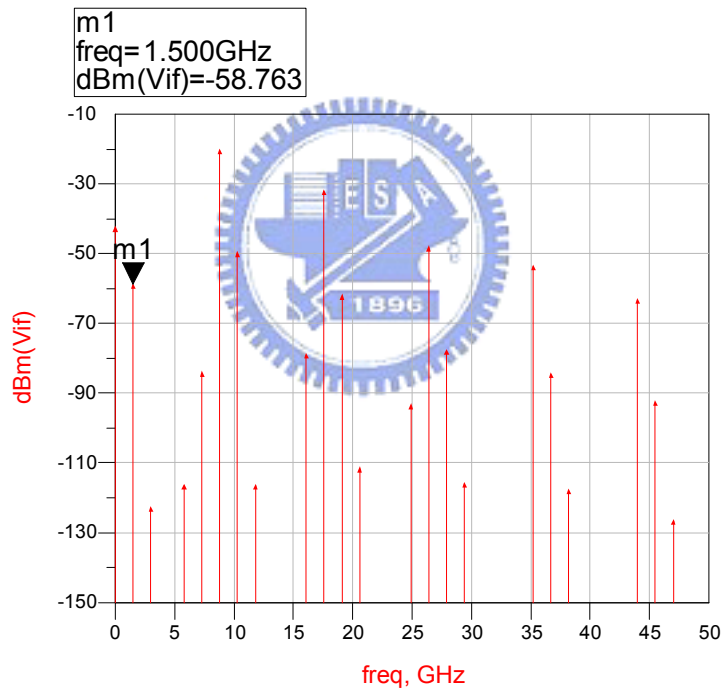
Fig. 4.1   Conventional very low intermodulation mixer

Fig. 4.2   The simulated spectrum of conventional VLIM when F_{LO} is 8.8GHz and F_{RF} is 10.3GHz without LO and RF filters

Conventional VLIM has many advantages. The most one is simple, and the others are no DC power consumption, no 1-dB compression point since it is a passive circuit. However, the LO and RF filters are essential for reducing intermodulation, such as shown in Fig. 4.2.

Fig. 4.3 shows a novel mixer, double balance very low

intermodulation mixer. Compared with conventional VLIM, its advantage is that **LO** and **RF** filters are not needed. The **LO** and **RF** signals would be eliminated by the symmetrical architecture.
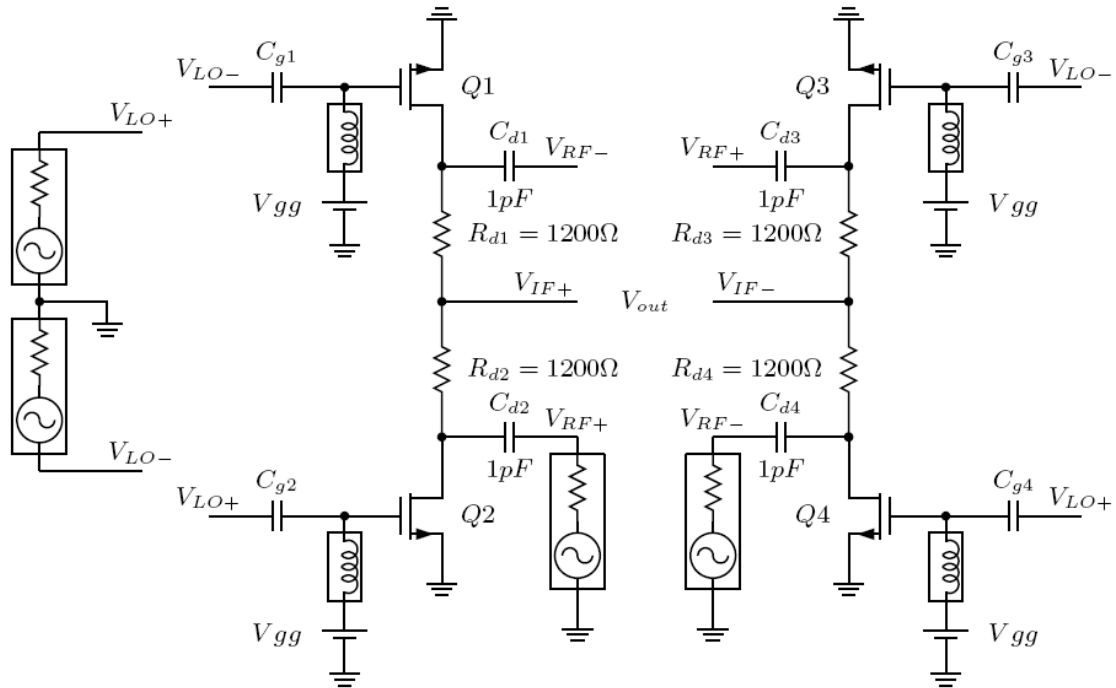

Fig. 4.3   Double balance very low intermodulation mixer
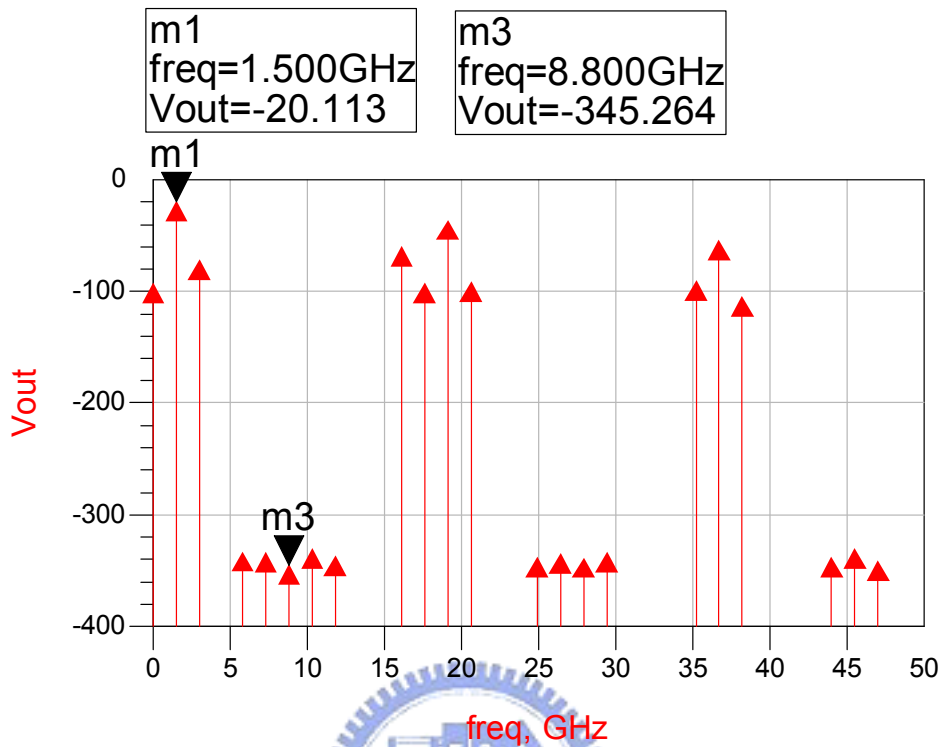
4.3 Simulated Results

Fig. 4.4   The output spectrum when F_{LO} is 8.8GHz and F_{RF} is 10.3GHz
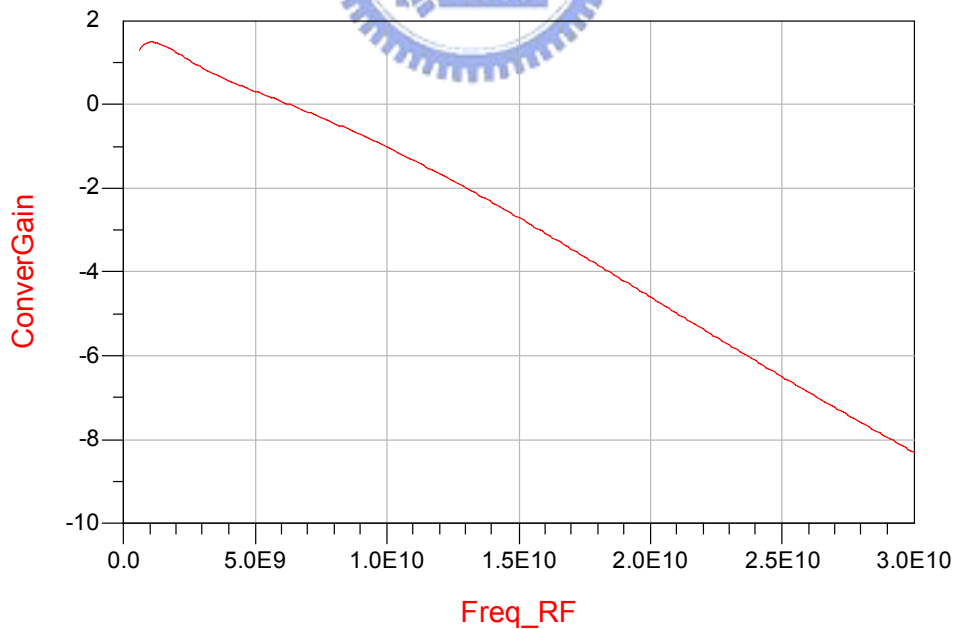

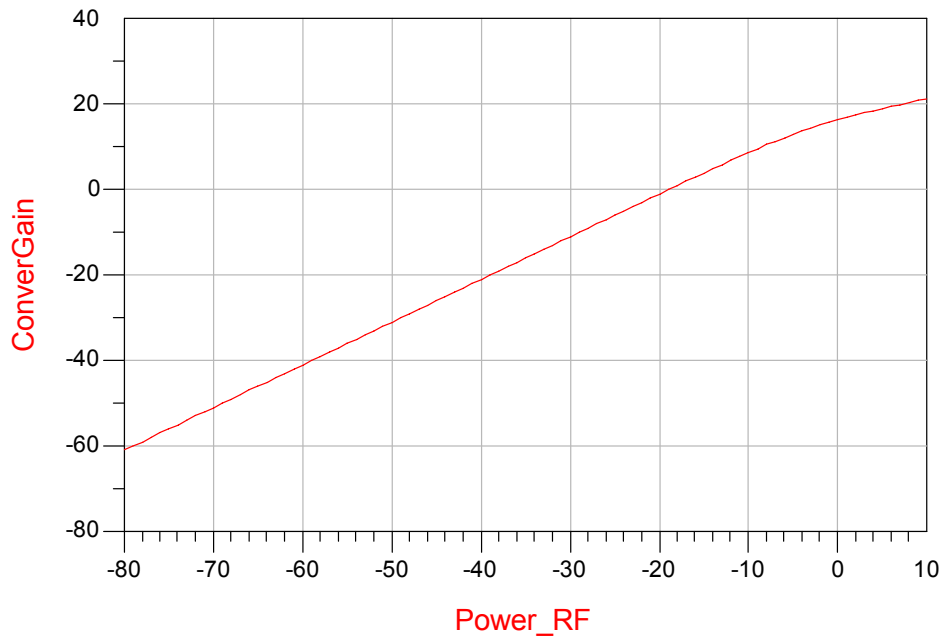Fig. 4.5   Conversion gain v.s. RF frequency when IF is 150MHz

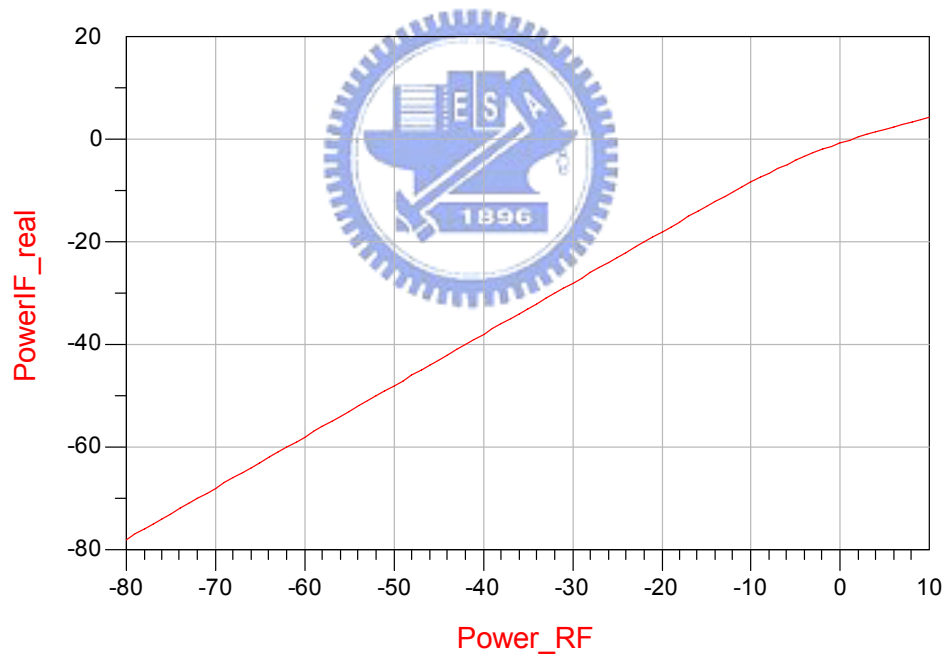Fig. 4.6　Conversion gain v.s. RF power when IF is 150MHz

Fig. 4.7　IF power v.s. RF power when IF is 150MHz

4.4　Conclusions For Double Balance VLIM mixer

A novel architecture of mixer is proposed. Its advantages are no DC power consumption, no *RF* and *LO* filters, and no 1-dB compression point since it is a passive mixer.

References

[1]   Y.-C. Ho et al., "3 V low noise amplifier implemented using 0.8 μm CMOS process with three metal layers for 900 MHz operation," Electron. Lett., vol. 32, pp. 1191–1193, June 1996.

[2]   G. Gramegna et al., "A 9-mW 900-MHz CMOS LNA with 1.05-dB noise figure," in Proc. Eur. Solid-State Circuits Conf., Stockholm, Sweden, Sept. 2000, pp. 112–115.

[3]   B. A. Floyd et al., "A 900-MHz 0.8 μm CMOS low-noise amplifier with 1.2-dB noise figure," in Proc. IEEE Custom Integrated Circuits Conf., San Diego, CA, May 1999, pp. 661–664.

[4]   A. N. Moheldin, E. Sanchez-Sinencio, and J. Silva-Martinez, "A 2.7-V 1.8-GHz fourth-order tunable LC bandpass filter based on emulation of magnetically coupled resonators," *IEEE J. Solid-State Circuits*, vol. 39, no. 7, pp. 1172–1181, Jul. 2003.

[5]   T. H. Lee, H. Samavati, and H. R. Rategh, "5-GHz CMOS wireless LANs,"*IEEE Trans. Microwave Theory Tech.*, vol. 50, no. 1, pp. 268–280, Jan. 2002.

[6]   Razavi, B., "A 2.4-GHz CMOS receiver for IEEE 802.11 wireless LANs," IEEE J. Solid-State Circuits, vol. 34, issue. 10, pp. 1382–1385, Oct. 1999.

[7]   M. N. El-Gamal, K. H. Lee, and T. K. Tsang, "Very low-voltage (0.8 V) CMOS receiver frontend for 5 GHz RF applications," *Proc. Inst. Elect. Eng. Circuits Devices Syst.*, pp. 355–362, Oct.–Dec. 2002.

[8]   J. W. M. Rogers and C. Plett, "A 5 GHz radio front-end with automatically Q tuned notch filter," in *Proc. IEEE BCTM*, 2002, pp. 69–72.

[9]   C. Y.Wu and C. Y. Chou, "A 5-GHz CMOS double-quadrature receiver front-end with single-stage quadrature generator," *IEEE J. Solid-State Circuits*, vol. 39, no. 3, pp. 519–521, Mar. 2004.

[10] Darabi, H. Khorram, S. Chien, E. Pan, M. Wu, S. Moloudi, S. Leete, J.C. Rael, J.J. Syed, M. Lee, R. Ibrahim, B. Rofougaran, M. Rofougaran, A., "A 2.4 GHz CMOS transceiver for Bluetooth" Radio Frequency Integrated Circuits (RFIC) Symposium, 2001. Digest of Papers. 2001 IEEE pp. 89-91, 2001.

[11] Trung-Kien Nguyen, " CMOS Low-Noise Amplifier Design Optimization Techniques" IEEE Trans. Microwave Theory Tech., vol. 52, pp. 1433–1442, May. 2004.

[12] Behzad Razavi, University of California, Los Angeles, "RF Microelectronics".

[13] Thomas H. Lee, Standford University, "The Design of CMOS Radio-Frequency Integrated Circuits".

[14] Jackson Harvey and Ramesh Harjani, "Analysis and Design of an Integrated Quadrature Mixer with Improved Noise, Gain, and Image Rejection," IEEE 2001.

[15] Woo, Y.Y.; Yang, Y.; Kim, B., "Analysis and Experiments for High-Efficiency Class-F and Inverse Class-F Power Amplifiers" IEEE Trans. Microwave Theory Tech., vol. 55, issue 5, pp. 1969- 1974, May. 2006.

[16] BERNARD SKLAR, Tarzana, California, "Digital Communications Fundamental and Applications", Second Edition, 2001.

[17] John G. Proakis, Northeastern University, "Digital Communications", Fourth Edition, 2001.

[18] Niklas Wadefalk, Anders Mellberg, Iltcho Angelov, Member, IEEE, Michael E. Barsky, Stacey Bui, Emmanuil Choumas, Ronald W. Grundbacher, Erik Ludvig Kollberg, Fellow, IEEE, Richard Lai, Niklas Rorsman, Piotr Starski, Senior Member, IEEE, Jörgen Stenarson, Student Member, IEEE, Dwight C. Streit, Fellow, IEEE, and Herbert Zirath, Member, IEEE, "Cryogenic Wide-Band Ultra-Low-Noise IF Amplifiers Operating at Ultra-Low DC Power", *IEEE Trans. Microwave Theory Tech.*, vol. 51, no. 6, pp. 1705–1711, Jun. 2001.

[19] Aly Ismail and Asad A. Abidi, Fellow, IEEE,"A 3–10-GHz Low-Noise Amplifier With Wideband LC-Ladder Matching Network," IEEE J. Solid-State Circuits, vol. 39, no. 12, pp. 2269–2277, Dec. 2004.

[20] Andrea Bevilacqua, Student Member, IEEE, and Ali M. Niknejad, Member, IEEE"AAn Ultrawideband CMOS Low-Noise Amplifier for 3.1–10.6-GHz Wireless Receivers" IEEE J. Solid-State Circuits, vol. 39, no. 12, pp. 2259–2268, Dec. 2004..

[21] Chang-Wan Kim, Min-Suk Kang, Phan Tuan Anh, Hoon-Tae Kim, and Sang-Gug Lee, "An Ultra-Wideband CMOS Low Noise Amplifier for 3–5-GHz UWB System", IEEE J. Solid-State Circuits, vol. 40, no. 2, pp. 544–547, Feb. 2005.

[22] Kyung-Wan Yu, Student Member, IEEE, Yin-Lung Lu, Da-Chiang Chang, Victor Liang, and M. Frank Chang, Fellow, IEEE, "K-Band Low-Noise Amplifiers Using 0.18 μ m CMOS Technology," *IEEE Trans. Microwave Theory Tech.*, vol. 14, no. 3, pp. 106–108, Mar. 2004.

[23]   K. B. Niclas, "The exact noise figure of amplifiers with parallel feedback and lossy matching circuits," IEEE Trans. Microwave Theory Tech., vol. MTT-30, pp. 832–835, May 1982.

[24]   STEPHEN A. MAAS, MEMBER, IEEE, "A GaAs MESFET Mixer with Very Low Intermodulation" IEEE Trans. Microwave Theory Tech., vol. MTT-35. NO.4, pp. 425–429, May 1987.

自傳

　　蔡順意，男，民國六十年七月六日生於臺灣省高雄市。民國八十二年六月畢業於臺灣科技大學電子工程系，並於同年入伍服役。退伍後，陸續服務於多家科技公司，目前任職於新竹科學園區智易科技股份有限公司，從事通訊網路產品研發。民國九十三年錄取交通大學電子工程研究所碩士班，從事射頻基體電路研究，指導教授為胡樹一博士。民國九十六年取得碩士學位。